Flood Hazard Assessment in Two Eastern Mediterranean Catchments Using a Multi-Indicator Approach

Despina Giannadaki , Antonis Bezes , Vassiliki Kotroni , Konstantinos Lagouvardos , Katerina Papagiannaki , Christina Oikonomou * , Haris Haralambous

Posted Date: 18 May 2026

doi: 10.20944/preprints202605.1112.v1

Keywords: flood hazard; analytic hierarchy process; multi criteria decision analysis; historical floods; weather intensity; Mediterranean catchments

 doi:10.20944/preprints202605.1112.v1

Article

Flood Hazard Assessment in Two Eastern Mediterranean Catchments Using a Multi-Indicator Approach

Despina Giannadaki [1], Antonis Bezes [2], Vasiliki Kotroni [2], Kostas Lagouvardos [2], Katerina Papagiannaki [2], Christina Oikonomou [1,3,*] and Haris Haralambous [3,4]

[1] CLOUDWATER Ltd., Agiou Ilarionos, 57, 1026 Nicosia, Cyprus
[2] National Observatory of Athens, Institute for Environmental Research and Sustainable Development; Penteli, Athens, 15236, Greece
[3] Frederick Research Center, Gianni Freiderikou 7, 1036 Nicosia Cyprus
[4] Frederick University, Gianni Freiderikou 7, 1036 Nicosia, Cyprus
* Correspondence: res.ec@frederick.ac.cy

Abstract

Floods triggered by intense precipitation represent one of the most significant natural hazards affecting Mediterranean regions, where complex terrain, rapid hydrological response and increasing urbanization can amplify flood impacts. This study presents a flood hazard assessment for two representative Eastern Mediterranean catchments: the Koiliaris River Basin in Crete-Greece and the Pediaios River Basin in wider Nicosia region in Cyprus. A composite Flood Hazard Index was developed by integrating three indicators representing key drivers of flood generation: the Topographic Wetness Index describing terrain-driven water accumulation, the Curve Number representing runoff potential, and the R20 precipitation frequency index. Spatial datasets including EU-DEM elevation data, CORINE land cover, European soil databases and precipitation information from the Copernicus CERRA reanalysis were used to derive the indicators. Each indicator was classified using the Natural Breaks method and combined through a weighted multi-criteria approach based on the Analytic Hierarchy Process. The resulting maps identify high-susceptibility areas mainly along river corridors and low-lying zones with high runoff and accumulation potential. Higher hazard levels occur in downstream areas of Koiliaris and urbanized zones of the Pediaios basin, particularly around Nicosia. Historical flood events were also analyzed to validate the index and examine links between rainfall intensity and impact severity.

Keywords: flood hazard; analytic hierarchy process; multi criteria decision analysis; historical floods; weather intensity; Mediterranean catchments

1. Introduction

Floods represent one of the most frequent and destructive natural hazard worldwide, causing extensive economic losses, disruption to infrastructure and significant threats to human safety. In recent decades, the frequency and intensity of flood events have intensified due to a combination of climate change, land-use change and increasing urbanization in flood-prone areas [1–3]. Flood impacts severity is affected by the rainfall characteristics (i.e., frequency, intensity, and duration), catchment characteristics, and the exposure and vulnerability of ecosystems and societies [4–6]. In Europe, and particularly in Mediterranean environments, hydrometeorological conditions favor the development of intense precipitation episodes capable of generating rapid runoff and flash flooding. The Mediterranean basin is characterized by pronounced climatic variability, steep terrain and strong

 doi:10.20944/preprints202605.1112.v1

land–sea contrasts, conditions that enhance the likelihood of short-duration high-intensity rainfall events and rapid hydrological responses in small to medium-sized catchments [7]. These characteristics make Mediterranean river basins particularly vulnerable to flash floods and associated societal impacts [8–12].

Effective identification of flood-prone areas is a critical component of disaster risk reduction and water resources management. Several approaches have been developed to assess flood hazards, ranging from physically based hydraulic simulations to spatial susceptibility modelling techniques. Physically based hydraulic models can provide detailed simulations of flood depth and inundation extent. However, their application typically requires high-resolution topographic data, detailed boundary conditions and long hydrometeorological records, which are not always available for many river basins [13–15].

Consequently, spatial flood susceptibility approaches have become widely used for preliminary hazard assessment and regional screening of flood-prone areas. These approaches aim to identify areas where flooding is more likely to occur by analysing environmental factors that influence runoff generation and water accumulation. Advances in geospatial data availability and spatial analysis techniques over the past two decades have significantly improved the capacity to conduct such assessments. Geographic Information Systems (GIS), combined with remote sensing datasets, enable the integration of geomorphological, hydrological and climatic information within a spatial modelling framework and are therefore widely used for flood hazard and flood susceptibility mapping [16–18].

Within GIS-based flood susceptibility modelling, multi-criteria decision analysis (MCDA) approaches are frequently applied to combine heterogeneous environmental indicators influencing flood occurrence. Among these techniques, the Analytic Hierarchy Process (AHP) is one of the most widely used methods for deriving weighting schemes among conditioning factors and constructing composite hazard indices. Numerous studies have demonstrated the effectiveness of GIS-AHP frameworks for identifying flood-susceptible zones and supporting spatial planning and risk assessment, particularly in data-limited environments [19–23].

Flood generation processes are controlled by a combination of geomorphological, hydrological and meteorological factors. Terrain characteristics strongly influence runoff pathways and water accumulation patterns within a catchment, while soil properties and land-cover conditions regulate infiltration capacity and surface runoff generation. Topography-derived indices are therefore frequently used in flood susceptibility modelling to represent the spatial distribution of potential water accumulation [24–26]. One of the most widely applied indicators is the Topographic Wetness Index (TWI), which describes the potential for soil moisture accumulation as a function of upslope contributing area and local slope gradient. Complementary to topographic controls, land-surface properties play a key role in determining runoff generation. The Curve Number (CN) indicator, originally developed by the Soil Conservation Service, remains one of the most widely applied empirical methods for representing the combined influence of soil infiltration capacity and land-use characteristics on rainfall-runoff processes [27]. Higher CN values typically correspond to reduced infiltration potential and increased surface runoff, conditions that are commonly associated with elevated flood susceptibility, particularly in urbanized environments where impervious surfaces dominate [28]. In addition to terrain and land-surface characteristics, the occurrence of flooding is strongly influenced by the frequency and intensity of extreme precipitation events. Climate extreme indices derived from long-term precipitation records provide a useful means of characterizing the spatial variability of heavy rainfall conditions capable of triggering floods. Indicators such as the annual number of days with precipitation exceeding specific thresholds have been widely used in climate impact studies to represent the climatological frequency of heavy rainfall events [29–33]. Integrating such indicators within flood hazard assessments allows the representation of both the hydrological response of the terrain and the meteorological forcing responsible for flood initiation [19,27,34].

 doi:10.20944/preprints202605.1112.v1

Beyond the application of these key indicators representing the main controls of flood generation, the analysis of historical flood events provides an essential complementary perspective for understanding flood hazard conditions. Databases documenting past flood events and their associated impacts provide valuable information on the temporal variability, seasonal patterns and severity of flood events. The integration of historical event analysis with spatial hazard modelling has been increasingly recognized as an important approach for interpreting flood susceptibility patterns and validating hazard assessment results [27,35–37]. Event-based analyses can effectively reveal relationships between rainfall intensity and observed impacts [11,38], while also providing insight into the temporal distribution of flood events within a region. Such information is particularly valuable for identifying periods of elevated flood activity and for enhancing the understanding of the interaction between meteorological forcing and catchment response.

Despite the growing number of studies focusing on flood susceptibility mapping, comprehensive assessments remain relatively limited for many river basins in the Eastern Mediterranean region. Catchments in this region exhibit strong hydro-climatic contrasts, ranging from mountainous watersheds with rapid hydrological responses to semi-arid basins characterized by intermittent flow regimes and significant urban influence. These characteristics complicate flood hazard assessment and highlight the need for integrated approaches that combine geomorphological, hydrological and climatological information. Relatively recent studies conducted in Mediterranean environments have demonstrated the value of multi-criteria approaches for identifying flood-prone zones and supporting regional flood risk analysis [20,34,39]. To cover the gap, this study develops a spatial flood hazard assessment for two representative Eastern Mediterranean catchments: the Koiliaris River Basin in Crete (Greece) and the Pediaios River Basin in Cyprus. A composite Flood Hazard Index (FHI) is constructed by integrating three indicators representing key controls of flood generation: terrain-driven water accumulation potential, runoff generation capacity, and the climatological frequency of intense rainfall events. The analysis combines geospatial datasets derived from digital elevation models, land-cover and soil information, and long-term precipitation reanalysis products. In addition, historical flood events in the surrounding regions are examined to characterize the temporal patterns and impacts of flood occurrence. By integrating multi-indicator spatial modelling with historical event analysis, the study provides a framework for identifying flood-prone areas and interpreting flood hazard patterns in contrasting Mediterranean catchments.

Next, Section 2 describes the study areas, datasets, and methodology used to derive the Flood Hazard Index (FHI) and analyze historical flood impacts. Section 3 presents the results, while Section 4 provides the main conclusions and future perspectives.

2. Materials and Methods

2.1. Description of the Study Catchments

The spatial flood hazard assessment is conducted for two river basins in the Eastern Mediterranean region: the Koiliaris River Basin in Crete, Greece, and the Pediaios River Basin in the Nicosia region of Cyprus. These watersheds represent characteristic Mediterranean catchments that are frequently exposed to high-intensity precipitation events capable of generating rapid runoff and flash flooding. Their selection provides representative examples of mountainous and semi-arid Mediterranean hydrological environments. Both basins exhibit hydrological responses that are strongly influenced by terrain characteristics, land-use patterns and rainfall variability. The Koiliaris basin represents a relatively small mountainous watershed with a well-monitored hydrological system, while the Pediaios basin represents a larger drainage system with significant urban influence and intermittent flow conditions.

Koiliaris River Basin (Crete, Greece)

The Koiliaris River Basin is located in the Chania regional unit in western Crete and flows from the northern slopes of the Lefka Ori mountain (White Mountains) towards the Cretan Sea (Figure 1).

 doi:10.20944/preprints202605.1112.v1

The watershed covers an area of approximately 130 km² and exhibits strong elevation gradients, with mountainous terrain exceeding 2000 m in the southern part of the basin and lower-lying agricultural areas in the northern coastal zone [37,40]. The geomorphological characteristics of the basin strongly influence its hydrological behaviour. The upstream mountainous region is dominated by steep slopes and highly permeable carbonate formations, while downstream areas consist of alluvial deposits and cultivated plains. Several tributaries originating from the mountainous terrain converge to form the main channel of the Koiliaris River, which flows northwards before discharging into the Cretan Sea near the village of Kalives. Land use within the basin is mainly characterized by agricultural activities, shrublands and limited forested areas, while rural settlements are located primarily in the lower and middle parts of the watershed. The combination of steep topography and episodic high-intensity rainfall events typical of Mediterranean climates can generate rapid surface runoff and significant increases in river discharge. As a result, the basin has been widely used as a natural laboratory for studying hydrological processes and flood generation mechanisms in Mediterranean environments [40].

The Koiliaris basin has also been the focus of several hydrological monitoring and modelling studies due to the availability of meteorological and discharge observations. These characteristics make the basin particularly suitable for testing and calibrating distributed hydrological models. The Koiliaris watershed thus provides a representative mountainous Mediterranean catchment for investigating the hydrological controls on infiltration, runoff generation, and flow routing that influence flood hazard conditions [41].

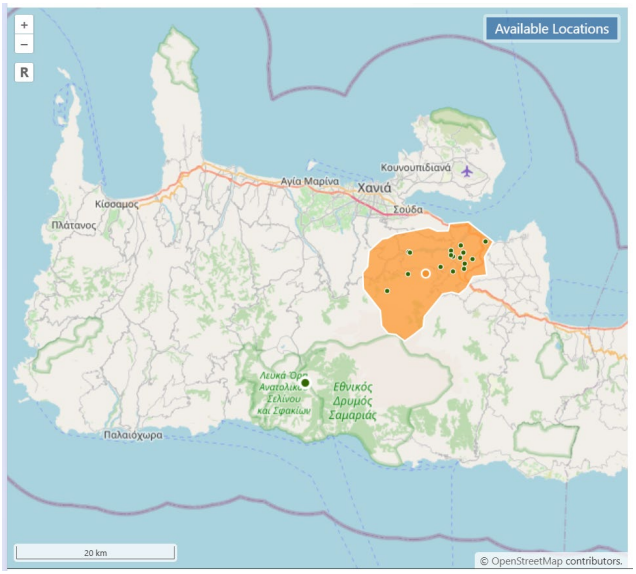

Figure 1. The Koilaris River Basin (Source map adapted from the Koiliaris Critical Zone Observatory webpage).

Pediaios River Basin (Cyprus)

The Pediaios River Basin is located in the central part of Cyprus and constitutes the longest river system on the island with total length of 98 km (Figure 2). The basin drains a large portion of the Nicosia district, extending from the Troodos foothills in the southwest towards the eastern coastal plains before ultimately reaching the area of Famagusta Bay [42].

The hydrological regime of the Pediaios River is typical of semi-arid Mediterranean environments. Streamflow is generally intermittent and highly dependent on seasonal precipitation patterns. During dry periods the river may exhibit limited or no continuous flow, while intense rainfall events during the wet season can produce rapid runoff and short-duration flooding episodes.

 doi:10.20944/preprints202605.1112.v1

These characteristics are further influenced by the basin's heterogeneous land-use patterns and the presence of highly urbanized areas within the Nicosia metropolitan region.

The Pediaios River has shaped Nicosia's urban evolution for centuries, characterized by a transition from its medieval course through the city center to its 16th-century diversion, a move prompted by a history of catastrophic flood events. Despite historical efforts to divert the Pediaios and manage its flow, Nicosia's modern urban expansion plays a significant role in shaping the hydrological response of the basin [43]. The expansion of impervious surfaces within the urban environment reduces infiltration and accelerates surface runoff, increasing the potential for localized flooding during intense rainfall events. In addition, the river channel has undergone significant modifications within the urban section of Nicosia, including channelization and flood-protection works, which alter the natural flow dynamics of the system [42].

The Pediaios watershed is a representative example of intermittent Mediterranean basins, where urban development and limited hydrological data introduce additional challenges for flood hazard assessment.

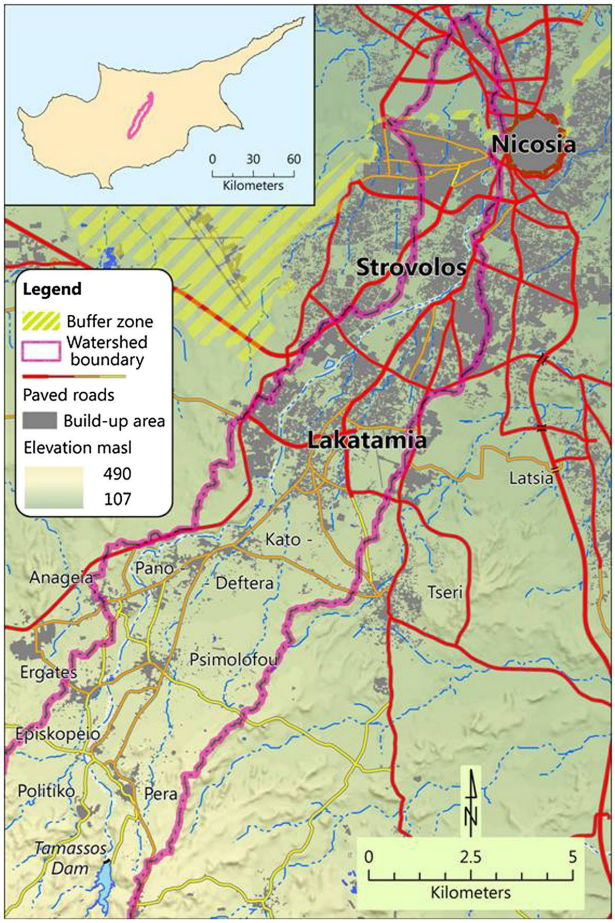

Figure 2. The Pediaios River Basin [43].

2.2. Flood Hazard Indicators and Input Data

Flood occurrence in river catchments is controlled by a combination of geomorphological, hydrological and meteorological factors. In order to characterize the spatial distribution of flood-prone areas within the study basins, a composite **Flood Hazard Index (FHI)** was developed based on the integration of three indicators determine key processes of flood generation:

a. **Topographic Wetness Index (TWI),** an indicator represents the spatial distribution of potential soil moisture and water accumulation across the landscape, based on terrain shape and slope. It combines information about how much water flows toward a location and how steep the

 doi:10.20944/preprints202605.1112.v1

land is at that point. Topographic characteristics were derived from the EU-DEM digital elevation model, which provides elevation data at approximately 25 m spatial resolution across Europe. The DEM was used to compute terrain slope and flow accumulation, which were subsequently used to derive the TWI [24]. TWI It is defined as:

$$TWI = \ln\left(\frac{\alpha}{\tan\beta}\right) \quad (1)$$

where α is the specific catchment area (upslope contributing area per unit contour length) and β is the local slope angle. High TWI values indicate areas where water is more likely to accumulate due to large contributing areas and low slopes, conditions that favour soil saturation and surface runoff generation, while steeper areas usually have lower values and are generally drier. The index is widely used in hydrological modelling and flood susceptibility mapping as a proxy for terrain-controlled saturation potential [24,26].

b. **Curve Number (CN)**, an indicator developed by the Soil Conservation Service [44] and used to estimate the potential of runoff generation from rainfall events, based on the combined influence of land use, soil permeability, and surface conditions on infiltration and runoff processes. Higher CN values indicate lower infiltration capacity and therefore greater runoff generation potential, typically associated with impervious or poorly infiltrating surfaces, while lower values indicate higher infiltration potential and reduced runoff. Land-use information was obtained from the CORINE Land Cover (CLC) database, which provides harmonized land-cover classification across Europe. Soil characteristics were derived from datasets available through the European Soil Data Centre (ESDAC) and SoilGrids products. These datasets were combined to assign Hydrologic Soil Groups (HSG) representing soil infiltration capacity. The HSG classification was then integrated with land-use information to estimate the Curve Number (CN) parameter for each grid cell following the Soil Conservation Service methodology [45]. The CN value for each grid cell was determined by combining:

- **Hydrologic Soil Group (HSG)** describing soil infiltration capacity (groups A-D), and
- **Land Use/Land Cover (LULC)** classification.

The CN method has been widely applied in hydrological modelling and flood susceptibility analyses [46,47].

c. **Heavy rainfall frequency (R20),** a climate indicator representing the frequency of heavy rainfall events. It is defined as the annual number of days with daily precipitation exceeding 20 mm. Higher values of the R20 indicate regions with more frequent heavy precipitation events, which may increase the likelihood of flood-triggering conditions. This index belongs to the standardized climate extreme indices developed by the Expert Team on Climate Change Detection and Indices (ETCCDI) and is widely used for characterizing the frequency of heavy precipitation events [48]. For the present study, R20 values were calculated using daily precipitation totals from the Copernicus European Regional Reanalysis for Europe (CERRA) dataset. Daily precipitation totals were analysed for the period 1990–2020, allowing the calculation of climatological statistics of extreme rainfall events across the study areas [32,33,48].

The selection of these indicators follows common practice in flood susceptibility and hydrological hazard mapping studies, where topographic controls, runoff generation potential and extreme precipitation frequency are considered the primary drivers of pluvial and fluvial flooding [19, 27. 37]. By combining these complementary indicators, the developed index captures both the hydrological response of the terrain and the climatological forcing associated with extreme precipitation events. To ensure comparability between the three indicators, each variable was classified into five ordinal classes representing increasing flood susceptibility. The classification was performed using the Natural Breaks (Jenks) method, which identifies optimal class boundaries by minimizing variance within classes while maximizing variance between classes [49]. The Jenks classification method has been widely applied in environmental hazard mapping and spatial risk assessment studies because it provides statistically meaningful class boundaries based on the distribution of the data [50,51]. Following classification, each indicator was normalized into a scale ranging from 1 (very low contribution to flood hazard) to 5 (very high contribution).

 doi:10.20944/preprints202605.1112.v1

The methodological workflow for the Flood Hazard Assessment consists of four main steps: 1. preparation of spatial datasets; 2. derivation of flood hazard indicators; 3. classification and normalization of indicators – all spatial datasets were resampled and harmonized to a common spatial resolution in order to ensure consistency in the spatial analysis and allow the integration of the different flood hazard indicators; 4. integration of indicators through a weighted Flood Hazard Index. In addition, historical flood events were analysed to provide contextual information on flood occurrence in the study areas and to support the interpretation of the hazard assessment results. This approach allows the evaluation of whether the physical flood susceptibility patterns identified by the FHI correspond to areas historically exposed to impactful hydrometeorological events and provides insight into the interaction between rainfall forcing and catchment response in the two Mediterranean environments.

2.3. Flood Hazard Index

The Flood Hazard Index (FHI) was calculated by combining the three normalized indicators using a weighted linear combination approach:

$$FHI = w_{TWI}S_{TWI} + w_{CN}S_{CN} + w_{R20}S_{R20} \quad (2)$$

where:

S_{TWI}, S_{CN}, and S_{R20} represent the standardized classes of each indicator. The terms w_{TWI}, w_{CN}, and w_{R20} denote their corresponding normalized weighting coefficients, which sum to unity. The weighting coefficients were determined using the Analytic Hierarchy Process (AHP) methodology [52,53], a multi-criteria decision-making technique that decomposes the problem into a structured pairwise comparison framework. Each indicator was systematically compared in terms of its relative importance for flood generation, considering its role in runoff production, water accumulation, and rainfall forcing. Consistency of the pairwise comparison matrix was evaluated to ensure logical coherence of expert judgments (Consistency Ratio within acceptable thresholds), and the resulting eigenvector solution was normalized to obtain the final weights:

- Topographic Wetness Index (TWI): 0.45
- Curve Number (CN): 0.40
- Extreme precipitation frequency (R20): 0.15

TWI (0.45) carries the highest weight, as it represents the spatial tendency of water accumulation driven by terrain morphology, slope, and upstream contributing area. It is directly associated with soil saturation potential and surface runoff concentration pathways, making it a primary control on flood susceptibility.

CN (0.40) is assigned a slightly lower but comparable weight, reflecting its strong representation of infiltration capacity, land use/land cover conditions, and soil hydrologic properties. CN effectively captures runoff generation potential under rainfall events and is therefore a critical determinant of flood response.

R20 (0.15) receives the lowest weight, as it represents the frequency of extreme precipitation events rather than spatial runoff conditioning. While it functions as the primary triggering driver of flood events, its influence is modulated by the landscape's capacity to store or transmit water, which is already captured by TWI and CN.

The resulting FHI values were finally classified into five flood hazard categories, ranging from very low to very high flood hazard. This classification facilitates spatial interpretation of flood susceptibility patterns and supports comparative hazard assessment across the study area.

2.4. Historical Flood Events Analysis

The analysis of historical flood events in Chania region (Crete) and Nicosia region (Cyprus) was conducted to provide contextual information on flood occurrence in the study areas and to support the interpretation of the flood hazard assessment results. The investigation of past events provides insights into the hydrometeorological conditions leading to flooding, the spatial distribution of

 doi:10.20944/preprints202605.1112.v1

impacts and the overall hydrological response of the catchments. Historical flood events were identified through the analysis of meteorological observations, hydrological records and information retrieved from national and international databases. Additional information was obtained from meteorological station records, high-impact weather event databases and reports from local authorities and scientific studies. These sources allowed the identification of representative flood episodes affecting the study areas. The recorded impacts for both regions include effects on people (e.g., fatalities, injuries or people trapped), damage to buildings and infrastructure, disruptions in transport and utility networks, impacts on economic activities and public services and emergency response actions such as evacuations [10,12]. Each local event is classified using two ordinal indicators: (1) **Weather intensity (W)**, based on representative meteorological observations (e.g., rainfall thresholds); (2) **Impact severity (I)**, reflecting the seriousness of the observed consequences within the affected area. These indicators can facilitate a comparison between meteorological conditions and reported impacts and are applied in this study to analyze flood events within the Regional Unit of Chania (hereafter, Chania) and the wider region of Nicosia (hereafter Nicosia).

Historical Flood Events in the Chania Region

The analysis presented in this section is based on the High-Impact Weather Events Database (HIWE-DB) [10,12], a national inventory of weather-related hazardous events affecting Greece and their reported direct societal impacts, developed by the METEO Unit at the National Observatory of Athens. The database covers all events since 2000 and is systematically updated. In HIWE-DB, an event is defined as a meteorological occurrence that produces societal impacts within a specific time window in Greece and may affect more than one prefecture, often through different hazardous phenomena. For each affected prefecture, the database records a local event documenting the reference city (the most affected location), the hazardous phenomenon, representative meteorological observations and reported impact information derived primarily from systematic monitoring of national and local media sources. According to the HIWE-DB classification, rainfall-induced flooding events include both floods and flash floods. In the Chania region, the majority correspond to flash-flood-type events.

In the present study, high-impact weather events are classified using two complementary metrics. The first classification is based on the severity of the meteorological conditions, while the second is defined by the type and severity of the impacts produced by the event. This approach enables the analysis of events with emphasis on impact magnitude and its relationship with weather intensity. Three levels of impact (I) and weather intensity (W) are considered following the categorisation used by Papagiannaki et al. [10,12] and presented in Table 1.

Events were categorized into the three intensity levels based on the magnitude of reported impacts and their geographical extent. This classification excludes direct economic costs due to data unavailability. The assessment accounts for a diverse range of consequences, specifically including human casualties and injuries, as well as disruptions to daily societal functions such as transportation networks and educational operations. Additionally, the criteria incorporate physical damage to private assets (e.g., vehicles and buildings) and public infrastructure, particularly electricity and telecommunication networks. The severity of the impacts is also evaluated in relation to the number of affected prefectures. Therefore, **I1 (low Intensity level)** represents small-scale problems restricted to a single prefecture; **I2 (medium Intensity level)** encompasses large-scale problems affecting 2-4 prefectures, significant disruptions in major urban centers, or verified lightning-induced fires; and **I3 (high Intensity level)** corresponds to severe impacts characterized by human fatalities, widespread damage across five or more prefectures, or prolonged societal disruption (e.g., transport outages) lasting more than three days.

Parallel to the impact classification, weather intensity levels were established as described in Table 1 and Papagiannaki et al. [10,12]. Historical data limitations – specifically inconsistent record lengths and the sparse geographical coverage of older stations – made not feasible the use of objective climatological thresholds for defining weather extremes. The subjective criteria we adopted from

 doi:10.20944/preprints202605.1112.v1

Papagiannaki et al. [10,12] were informed by the MEDEX project [54], as shown in Table 1, and is presumed to maintain the integrity of the results. Events are classified based on whether they meet at least one threshold or observe a specific phenomenon within a given intensity category.

Table 1. Criteria used for the classification of **impact severity (I)** and **weather intensity (W)** at the local-event level adapted for Chania and Nicosia regions.

Impact Severity (I)			
Level	**I1 – Low**	**I2 – Moderate**	**I3 – High**
	Minor disruptions and light damage (e.g., in transportation, telecommunications/electricity networks, buildings, and infrastructure) within the affected prefecture	Serious damage and large-scale disruption within the affected prefecture	Human losses, and/or widespread disruptions/damages that continue to affect the prefecture after the end of the weather event
Weather Intensity (W)			
Level	**W1 – Low**	**W2 – Moderate**	**W3 – High**
Chania	Rainfall < 60 mm/24h or <15 mm/1h	Rainfall 60–100 mm/24h or 15-25 mm/1h	Rainfall > 100 mm/24h or >25 mm/1h
Nicosia	Rainfall < 55 mm/24h	Rainfall 55–89 mm/24h	Rainfall > 89 mm/24h

Historical Flood Events in the Nicosia Region

The methodology was adapted for the Nicosia region to account for the specific administrative and climatological context of Cyprus while maintaining fundamental consistency with the HIWE-DB framework. This analysis integrates two primary datasets spanning the 26-year period from 2000 to 2025, 1. Historical flood records, and 2. Rainfall data. Historical flood records for the Nicosia region (2000–2025) were obtained from the Cyprus Water Development Department (WDD) [55]. This dataset provides a systematic inventory of rainfall-induced flooding, documenting the timing, locations, hydrological details like river overflows, and meteorological metadata for the most recent events. A key feature of this registry is the use of multiple sources such as Fire Service reports, WDD technical records, newspaper archives, and academic research, to reconstruct each event's impacts. By integrating these diverse sources, the dataset provides a comprehensive range of consequences, specifically including human health (injuries/fatalities), economic assets (damage to buildings and vehicles), and critical infrastructure (transportation and utility disruptions). We used these documented consequences and the reported geographical extent to categorize each event into one of three impact severity levels. Following this framework, we categorized impact severity (I levels) for Cyprus based on the magnitude of the consequences as in Chania case study, and their spatial distribution across the island's administrative districts. Therefore, similar to Chania I1 (Low Severity level) represents localized events with minor disruptions and light damages; I2 (Medium Severity level) corresponds to events causing significant disruptions in urban centers or have a broader geographical extend to more than one district; and I3 (High Severity level) represents events with the most severe impacts including human fatalities which have a broader geographical extend and prolonged disruptions.

To complete the analysis weather intensity levels were adapted for the Nicosia region to reflect the climatological characteristics of Cyprus. High-resolution rain data were obtained from the Cyprus Department of Meteorology (DoM) to derive local high-intensity weather threshold. The dataset comprises 10-minute interval measurements aggregated into 24-hour totals for the period 2000-2025 (26 years). In total, 9,180 daily records for the Nicosia urban area were analysed, of which approximately 74% correspond to zero-rainfall days, highlighting the strongly seasonal and

 doi:10.20944/preprints202605.1112.v1

intermittent precipitation regime typical of the semi-arid climate of the region. In this context, the threshold for the highest weather-intensity level (W3) was defined using the 99.9th percentile of the daily rainfall distribution. For the Nicosia dataset, this corresponds to **89 mm in 24 h**, representing events that occur on average only **0.4 times per year** (10 events in the entire record or roughly once every 2.5 years). The use of the 99.9th percentile (instead of the 99th percentile corresponding to ~30 mm/24 h) ensures that the W3 class captures only exceptionally rare and potentially hazardous precipitation events and is considered a more appropriate threshold for defining extreme precipitation within the semi-arid climatic conditions of Cyprus. The selected thresholds are also consistent with the operational warning criteria of the Cyprus DoM, providing an additional policy-based justification. Although the DoM defines a Red Alert for 115 mm in 24 h, red warnings are also issued when rainfall exceeds 90 mm within 3 hours. In semi-arid Mediterranean regions, extreme daily totals are typically generated by short-duration, high-intensity convective storms. Therefore, a daily accumulation approaching 89 mm likely implies that a substantial fraction of the rainfall occurred within a few hours, potentially reaching the operational criteria for severe weather warnings. While the threshold for the W3 level is defined based on the statistical extreme of the rainfall distribution, the lower and intermediate intensity classes were defined to maintain consistency with operational warning thresholds of DoM. The threshold for low weather intensity W1 was set at 55mm. While this value exceeds the 99th percentile (30mm) of the 26-year daily series for Nicosia, it was selected to ensure consistency with the Cyprus Department of Meteorology's "Yellow Alert" criteria (daily rain over 55mm/24h). By setting W1 at this level, the analysis focuses exclusively on impactful events that necessitate public awareness or civil intervention. The intermediate class (W2) therefore covers rainfall totals between **55 mm and 89 mm**, corresponding broadly to events associated with Yellow and Orange alerts [56]. Table 1 presents the impact intensity (I) and weather severity (W) for Nicosia. The resulting classification integrates local climatological statistics with the operational warning thresholds of the Cyprus Department of Meteorology, ensuring that the defined rainfall categories capture events that are both statistically extreme and operationally relevant for the Nicosia region.

3. Results

3.1. Flood Hazard Analysis for the Study Catchments

The Flood Hazard Index (FHI) was calculated for the two studied basins, the Koiliaris River Basin in Crete (Greece) and the Pediaios River Basin in Nicosia, Cyprus, by combining the three standardized indicators described in the methodology section (equation 2). The resulting FHI values provide a spatial representation of potential flood hazard conditions across the study areas, highlighting locations where terrain characteristics, runoff potential and rainfall triggering conditions combine to increase the likelihood of flood generation.

3.1.1. Flood Hazard Index Results for Koilaris River Basin

The spatial distribution of the FHI for the Koiliaris River Basin is presented in Figure 3. The results indicate a clear spatial pattern linked to the geomorphological structure of the basin. Areas characterized by moderate to high flood hazard are primarily located along the main river corridor and in the lower parts of the basin where surface runoff from the mountainous upstream areas converges. These areas are characterized by relatively high TWI values, indicating increased water accumulation potential. The spatial distribution of the FHI confirms the effectiveness of the AHP-weighted multi-indicator approach. By assigning the highest weight to the TWI (0.45) and CN (0.40), the model successfully identifies the coastal plains north in the region as critical accumulation zones. This pattern reflects the hydrological behaviour of the Koiliaris basin, where steep mountain slopes upstream cause water to run off quickly, eventually collecting in the flat farmland and coastal plains downstream. Simultaneously, the lower weight assigned to R20 (0.15) is sufficient to highlight the mountainous upstream areas in the south of the basin as essential runoff-contributing areas.

 doi:10.20944/preprints202605.1112.v1

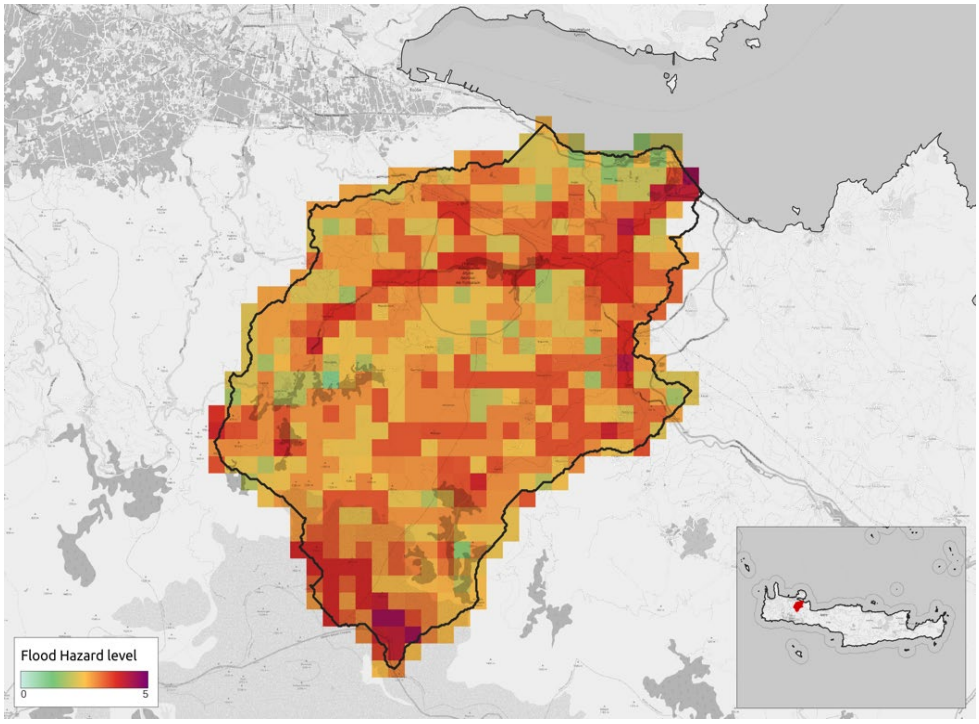

Figure 3. Flood Hazard Index for the Koiliaris River Basin.

3.1.2. Flood Hazard Index Results for Pediaios River Basin

The Flood Hazard Index for the Pediaios River Basin is presented in Figure 4. In contrast to the geomorphologically driven hazard patterns observed in Koilaris, the Pediaios basin exhibits a hazard profile heavily influenced by anthropogenic activity. Areas of elevated flood hazard are mainly located along the main course of the Pediaios River and its tributaries, particularly in sections crossing the Nicosia urban area, in the northern part of the catchment. In these areas, the combination of relatively high CN values associated with urban land cover contribute significantly to the elevated flood hazard index. While the R20 index was assigned a low weight of 0.15 in the AHP matrix, its role is functionally significant; it acts as the climatological trigger that activates the high runoff potential of the impervious urban surfaces. While the index is primarily governed by the basin's physical characteristics – specifically land cover and topography – the 15% weighting of the R20 index provides a critical climatological modulation. This ensures that the final FHI reflects not only the physical susceptibility of the Nicosia metropolitan area but also the frequency of the actual hydrometeorological forcing required to trigger a flood event. This pattern reflects the hydrological behavior of an urbanized semi-arid system: the expansion of impervious surfaces reduces natural infiltration and accelerates surface runoff, making the metropolitan region highly sensitive to episodic rainfall events. Conversely, the analysis also reveals that upstream regions of the basin are characterized by low flood hazard levels. This is attributed to lower upslope contributing areas and relatively lower runoff potential in the foothills, where the absence of dense urbanization allows for higher infiltration compared to the downstream urban area.

 doi:10.20944/preprints202605.1112.v1

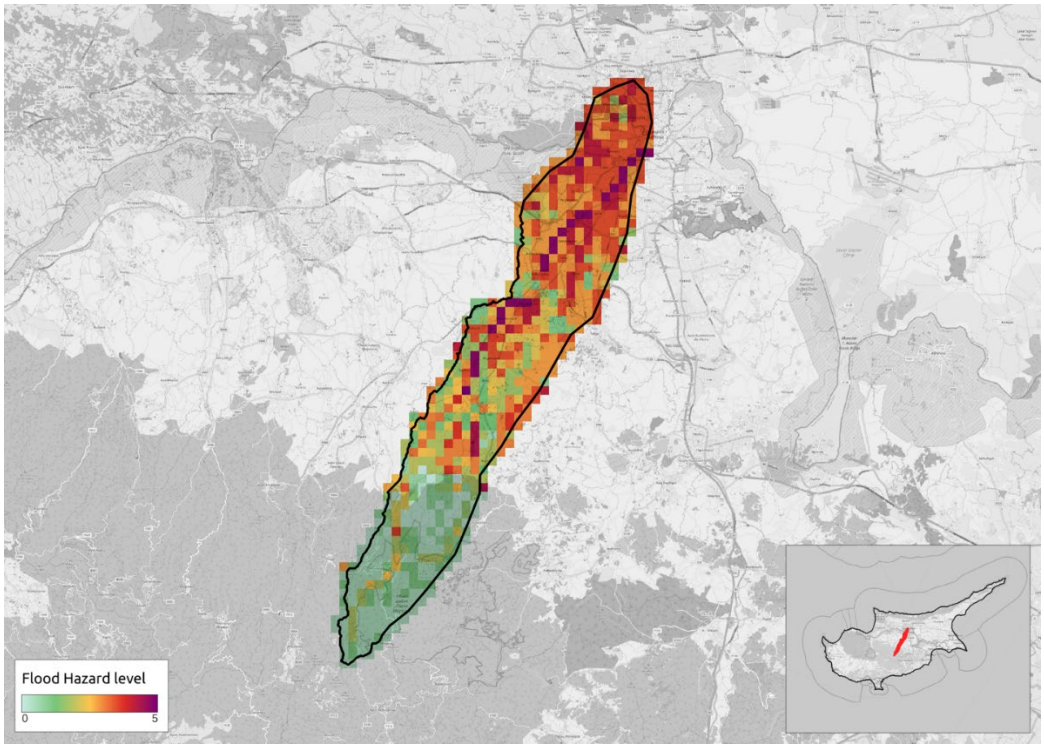

Figure 4. Flood Hazard Index for the Pediaios River Basin.

3.2. Validation of Flood Hazard Patterns Through Historical Event Analysis

While the FHI provides a spatial representation of potential flood susceptibility based on geomorphological, hydrological and climatological indicators, the examination of past flood events offers an important empirical perspective for interpreting these results. Historical flood records provide information on the meteorological conditions that have led to flooding in the past, the temporal distribution of events and the magnitude of their impacts. Integrating historical event analysis with spatial hazard modelling therefore allows the assessment to move beyond "theoretical" susceptibility and examine how the identified hazard patterns relate to documented flooding episodes and their associated consequences.

In this study, historical flood events affecting the broader areas surrounding the Koiliaris River Basin in Chania and the Pediaios River Basin in Nicosia are analysed to provide temporal and impact-based context for the spatial hazard patterns identified in the previous sections. The analysis focuses on the frequency, seasonal distribution and impact severity of documented flood events, as well as their relationship with rainfall intensity.

3.2.1. Historical Trends and Impact Severity in Chania Greater Area

The analysis of the HIWE-DB for the Chania region identified 37 flood-related events between 2000 and 2025. This number exceeds the national mean number of flood events per prefecture in Greece (21 events), indicating a relatively high frequency of flood-related hazards in the region. The distribution of impact severity shows that most events were classified as **low (I1)** or **moderate (I2)** severity, each representing approximately 43% of the total, while high-severity events (I3) account for 14% of the total. A complete list of recorded flood events affecting the area, including their dates, reference locations, impact severity classifications (I), and brief descriptions of reported impacts, is provided in Table 2. Despite the relatively limited number of high-impact events, flood-related hazards have resulted in two fatalities, accounting for one-third of the six weather-related fatalities recorded in the area during the study period. These high-severity events – defined by human fatalities, extensive infrastructure destruction, or prolonged societal disruption – consistently

 doi:10.20944/preprints202605.1112.v1

coincide with the "High" and "Very High" (Level 4–5) hazard classes derived from the multi-indicator FHI model. The spatial distribution of these high-impact flood events (I3) provides an empirical baseline for evaluating the model's performance across diverse physical environments. Specifically, the high-severity events in Maleme (October 2017), Platanias (December 2014), and the major road subsidence in Kalidonia (February 2003) occur within the modeled "Very High" hazard zones of the downstream alluvial plains. In these sectors, the FHI effectively integrates the convergence of high topographic water accumulation (TWI) and elevated surface runoff potential (CN), identifying these areas as critical nodes of infrastructure vulnerability. Similarly, the impacts documented in Vrysses (February 2019) and the Samaria Gorge (September 2024) align with the hazard levels identified in the basin-margin transition zones and steep drainage pathways. The results indicate that the FHI accurately accounts for the geomorphological drivers and land-surface characteristics that facilitate rapid surface runoff during extreme precipitation events. Finally, the historical record confirms that these I3 impacts were exclusively triggered during Weather Intensity Level W3 episodes (i.e., rainfall >100 mm/24h), suggesting that the FHI successfully identifies the specific physical environments where extreme meteorological forcing results in the most severe societal consequences.

The annual distribution of flood events, presented in Figure 5, reveals substantial interannual variability across the study period. During the early part of the record, several years occurred without documented flood events. However, from the early 2010s onward, the frequency of flood occurrences increased, with multiple years experiencing two or more events. The highest annual frequency occurred in 2019, with a total of six recorded flood episodes. This increase in event frequency may reflect a combination of improved reporting practices, increased susceptibility of flood-prone zones, and shifting precipitation regimes that may favor more frequent extreme weather events.

Flood occurrences in Chania also exhibit a pronounced seasonal pattern (Figure 6). Most events occur during the autumn and early winter months, which coincide with the period of highest precipitation intensity in the eastern Mediterranean. The highest event frequencies were recorded in October and November, with eight events each, followed by February (six events) and December (four events). In contrast, flood events are rare during late spring and summer, with no events recorded in July. This seasonal pattern is consistent with the regional climatology, where intense convective and frontal rainfall systems occur predominantly during the transition from the dry summer season to the wetter winter period. The two recorded flood-related fatalities occurred during February and September, indicating that severe impacts are not limited exclusively to the peak autumn season.

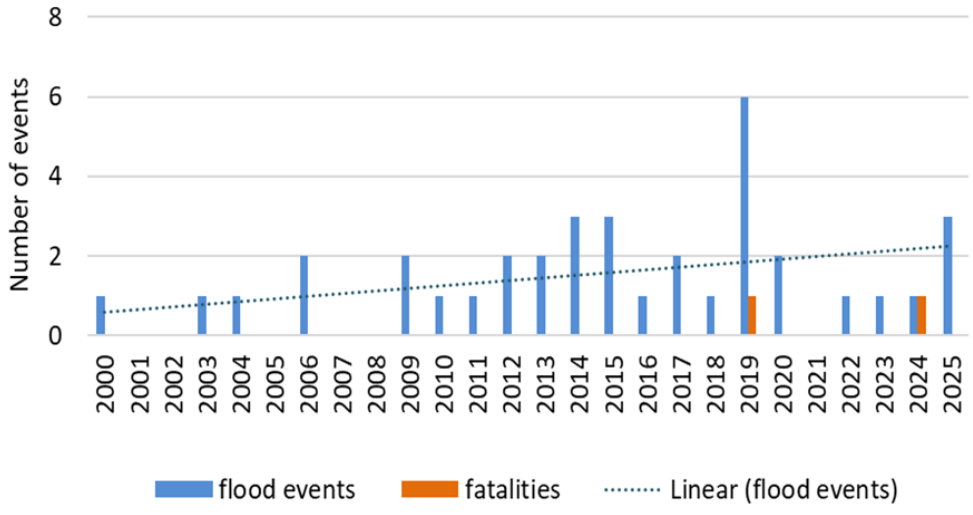

Figure 5. Annual distribution of flood events affecting Chania during the study period.

 doi:10.20944/preprints202605.1112.v1

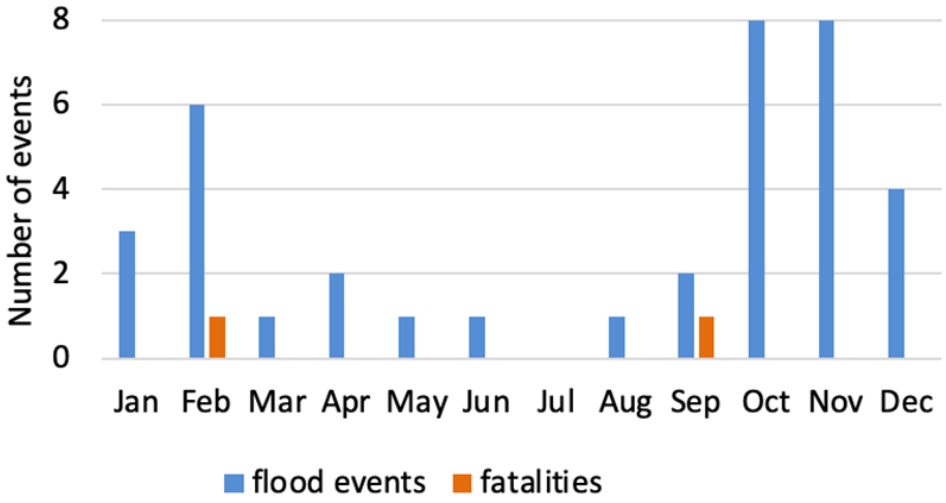

Figure 6. Monthly distribution of flood events affecting Chania during the study period.

The relationship between weather intensity (W) and impact severity (I) is illustrated in Figure 7. Events classified as low weather intensity W1 are predominantly associated with low impact severity I1 (over 60%). Moderate-intensity events W2 are evenly distributed between I1 and I2, indicating that moderate rainfall can still produce noticeable impacts depending on local conditions. In contrast, high-intensity events (W3) show a clear shift toward more severe consequences. Among the W3 events, eight were classified as I2 and four as I3 accounting for 70% of the total events. Notably, all high-severity impacts (I3) are exclusively observed under W3 conditions. This suggests that while W3 rainfall does not always result in maximum severity, it serves as a functional threshold and a necessary condition for triggering the most damaging flood episodes in the region.

Overall, the documented flood characteristics align with the terrain-driven hazard patterns identified throughout the study area. In environments such as the Koiliaris basin, the synergy between steep upstream gradients and low infiltration capacity drives the rapid hydrological response characteristic of mountainous Mediterranean catchments.

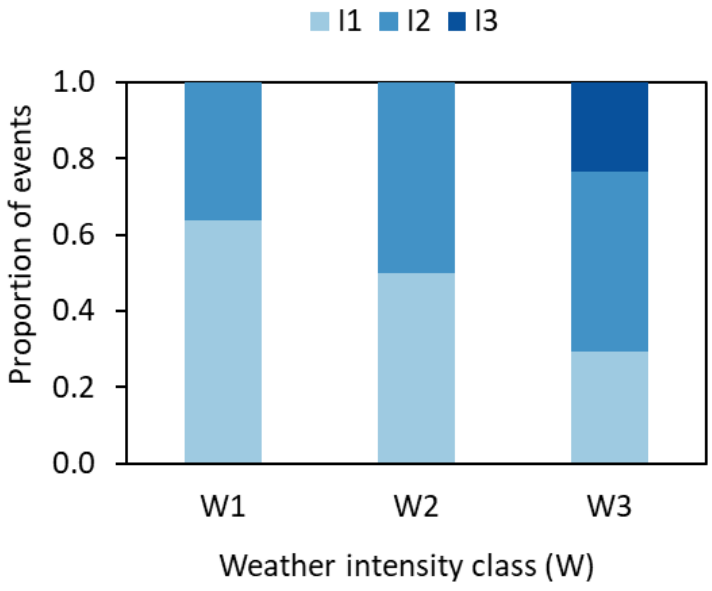

Figure 7. Distribution of flood events in Chania by impact severity (I) within each weather intensity class (W).

 doi:10.20944/preprints202605.1112.v1

Table 2. Flood events that affected Chania in 2000-2025. Data include date, reference location, impact severity (I), and a brief description of reported impacts (source: HIWE-DB).

Date	Reference area	I	Description
06-Nov-25	Chania Old Town	1	Flooding caused damage to businesses in Chania's Old Town.
01-Apr-25	Souda	1	Flooding with limited impacts recorded in Chania.
14-Jan-25	Chania	1	Flooding reported in Chania.
18-Sep-24	Samaria Gorge	3	A 33-year-old tourist died after a landslide triggered by heavy rainfall in Samaria Gorge; dozens of people required evacuation.
05-May-23	Chania Akrotiri	2	Mud torrents swept a driver in the Akrotiri area, causing road damage and impacts to businesses.
15-Oct-22	Stavros	1	Flood damage recorded in Stavros, Chania.
07-Dec-20	Asi Gonia	1	Flooding and debris flows occurred in Asi Gonia due to intense rainfall, endangering a livestock farmer.
22-Oct-20	Chania	2	Heavy rainfall caused flooding, landslides, debris flows, infrastructure damage, and power supply disruptions in northern Chania; people in Souda were endangered.
13-Nov-19	Alikianos	2	Severe impacts from heavy rainfall and strong winds, mainly in the Alikianos area.
10-Nov-19	Kissamos	2	Intense rainfall flooded houses and businesses in western Crete; vehicles were swept away, and residents in villages of Chania required rescue.
25-Feb-19	Vrysses	3	Storm "Oceanis": heavy rainfall caused severe flooding and destruction in western Crete, resulting in one fatality in Vrysses.
14-Feb-19	Platanias	2	Storm "Hioni": flooding and damage on the local road network of Platanias municipality.
05-Feb-19	Sfakia	1	Flooding reported in Sfakia.
01-Jan-19	Chania	2	Storm "Rafael": intense rainfall and landslides caused flooding in Chania.
20-Feb-18	Sfakia	2	Rainfall caused damage to road infrastructure in the Sfakia municipality.
26-Oct-17	Maleme	3	Storm "Daedalus" caused destructive flooding in Chania.
11-Feb-17	Chania	2	Heavy storms caused flooding in the city of Chania; a landslide damaged part of the Venetian fortification, and major damage occurred to the road network.
31-Oct-16	Vrysses	1	Heavy rainfall caused minor flooding and the collapse of an abandoned building.
26-Sep-15	Samaria Gorge	2	Sixty tourists were trapped in Samaria Gorge due to intense rainfall.
14-Aug-15	Chania	1	Urban flooding caused traffic disruptions in the city of Chania.
08-Jun-15	Kissamos	1	Landslide closed the national road between Kolymbari and Kissamos; flooding occurred in Chania streets.
30-Dec-14	Platanias	3	Prolonged rainfall caused severe floods and damaging landslides in Chania.
07-Nov-14	Kissamos	1	Flooding reported in Chania.
24-Oct-14	Samaria	2	Landslide closed the road to Petra–Seli and the Samaria National Park.
03-Dec-13	Kissamos	2	Flooding and strong winds caused landslides in Kissamos and other parts of Crete.
14-Nov-13	Kissamos	1	Severe weather caused problems mainly on the rural road network in the municipalities of Kandanos–Selino and Kissamos.
16-Nov-12	Kounoupidiana	2	Long power outages in Chania due to a storm and intense lightning.
30-Jan-12	Souda	2	Flooding and landslides caused problems on the Chania road network.
14-Nov-11	Samaria	2	Flooding and landslides affected the road network of Chania.
28-Dec-10	Chania	1	Storm caused flooding and transport disruptions in Chania.
24-Oct-09	Chania	1	Flooding reported in Chania.
05-Apr-09	Gavdos	1	Heavy rainfall caused flooding in Gavdos, damaging coastal infrastructure and roads.
17-Oct-06	Chania	1	Flooding reported in Chania.
12-Oct-06	Chania	2	Flooding reported in Chania.
05-Nov-04	Chania Airport	2	Severe storms in Crete caused flooding in Chania.
17-Feb-03	Kalidonia	3	Storms caused major road subsidence in the Kalidonia area of Chania.
20-Apr-00	Gavdos	1	Flooding in southwestern Crete left the island of Gavdos isolated.

 doi:10.20944/preprints202605.1112.v1

3.2.2. Historical Trends and Impact Severity in Nicosia Greater Area

The analysis of historical flood events in the Nicosia region, based on records from the Water Development Department (WDD) and rainfall data from the Cyprus Department of Meteorology, identified 58 flood-related events during the period 2000-2025. This relatively high number of recorded events highlights the pronounced flood activity in the Nicosia area, despite its semi-arid climatic setting. The distribution of impact severity indicates a clear dominance of low-severity events (I1), which account for approximately 59% of the total, followed by moderate-severity events (I2) at 33%, while high-severity events (I3) represent only 8% of the database (5 events in 26 years). A complete list of recorded events, including dates, affected locations, impact classifications, and reported consequences, is provided in Table 3. Although high-impact events are relatively infrequent, they account for the most severe societal consequences, including two recorded fatalities in 2003.

High-severity events (I3) are predominantly located within areas classified as "High" and "Very High" (Levels 4–5) by the FHI (see Figure 4), supporting its validity within the Pediaios basin. This pattern is most evident for events occurring in the urban areas of Nicosia. The December 2003 flood episodes (2 and 12-13 December) in urban areas and the outskirts of Nicosia, which resulted in fatalities, bridge failures, and widespread infrastructure disruption, were associated with overflows of the Pediaios, Gialias, and tributaries. These impacts are spatially aligned with the "Very High" FHI zones characterized by high TWI values (topographic convergence along river corridors) combined with elevated CN values reflecting dense urban impermeable areas. Similarly, the events of 31 May 2005 (Aglantzia, Lakatamia, Strovolos, Engomi) and 27 October 2009 (Alambra, Nisou, Lymbia, Dali), which caused extensive property damage, infrastructure disruption, and Pediaios and Gialias rivers overflows, occurred within areas identified by the model as critical flood hazard zones, spanning both densely urban and peri-urban parts of the basin. In contrast, the 20 October 2018 event (Kakopetria, Alambra) – classified as I3, primarily affected upstream, less urbanized areas. In the FHI map, Kakopetria area corresponds to moderate-to-high hazard classes driven mainly by topographic controls (elevated TWI) rather than urban runoff potential. This indicates a different flood-generating mechanism, dominated by rapid runoff in steep terrain under extreme rainfall, rather than the urban pluvial-fluvial interactions that characterize the Nicosia urban area. Overall, while I3 events within the urban areas consistently align with "Very High" hazard zones, cases such as Kakopetria highlight the model's ability to differentiate between geomorphologically driven and urban-driven flood regimes.

In contrast to terrain-driven systems such as Chania, the historical record in Nicosia highlights a flood regime strongly influenced by urban characteristics. The most severe impacts (I3) are associated with moderate and high-intensity rainfall events (W2 and W3), but their spatial distribution is primarily controlled by the urban environment rather than by geomorphology alone. The alignment between documented impacts in densely urbanized districts such as Old Nicosia, Strovolos, Lakatamia, and Engomi and the modeled high-hazard zones confirms that the FHI effectively captures areas where high surface runoff potential (i.e., CN) coincides with limited drainage capacity. This agreement indicates that the FHI successfully represents the transition from natural riverine flood processes to predominantly urban pluvial flooding conditions within the Pediaios basin.

The annual distribution of flood events, presented in Figure 8, reveals a relatively consistent baseline of flood occurrence throughout the study period. In contrast to Chania, where several early years show no recorded events, flood incidents in Nicosia are documented in nearly all years, with the exception of 2007. From the mid-2010s onward, a noticeable increase in event frequency is observed, with multiple years recording two or more events. The highest annual frequency occurred in 2018 (eight events), followed by 2019 (six events). This period of intensified activity coincides with similar peaks observed in Chania (Figure 5), suggesting a broader regional signal of increased hydrometeorological variability. In the case of Nicosia, this trend likely reflects a combination of improved reporting practices – following European Union guidelines, densifying urbanization, and a shift toward more frequent high-intensity convective rainfall events.

 doi:10.20944/preprints202605.1112.v1

The seasonal distribution of flood events in the Nicosia region (Figure 8) exhibits a clear pattern, with two distinct periods of elevated activity, in contrast to the more concentrated seasonality observed in the Chania region. Events are more frequent in the transitional seasons – spring and autumn, when conditions shift between wet and dry regimes – as well as in the mid-winter period, coinciding with peaks in precipitation intensity over Cyprus. The highest frequency is observed in December (ten events), followed closely by May, October, and January, each with nine recorded events. Flood events are rare during the height of summer, with no events recorded in August and only one event in July, while June has experienced 3 events in the 26-year period. This distribution reflects the semi-arid Mediterranean climate of inland Cyprus, where flood-generating rainfall occurs both during winter synoptic systems and spring–autumn convective outbreaks. Notably, the two recorded fatalities in Nicosia occurred in December, coinciding with the peak in event frequency and highlighting the elevated risk associated with wintertime precipitation extremes.

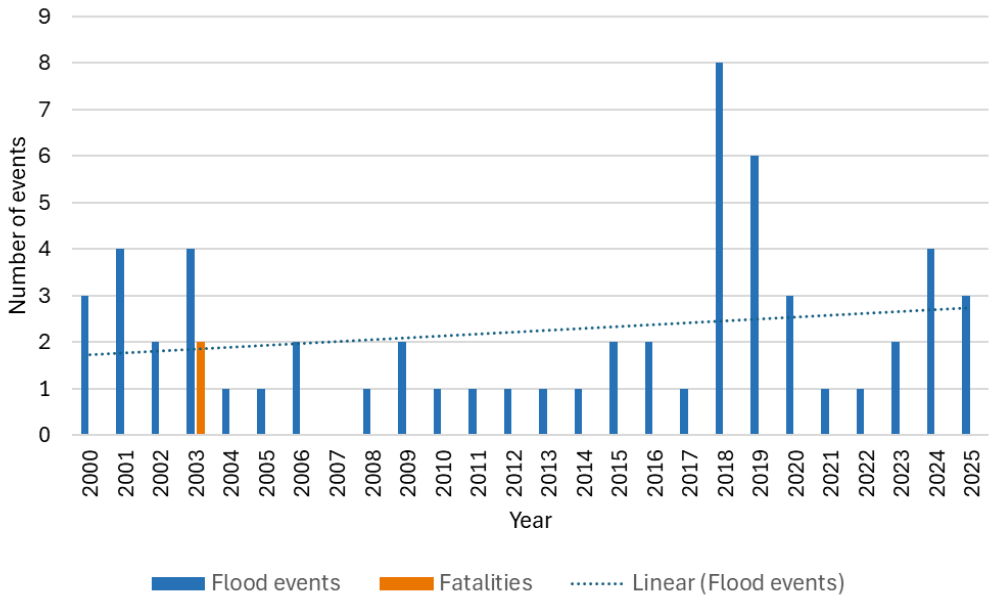

Figure 8. Annual distribution of flood events affecting Nicosia wider region during the study period.

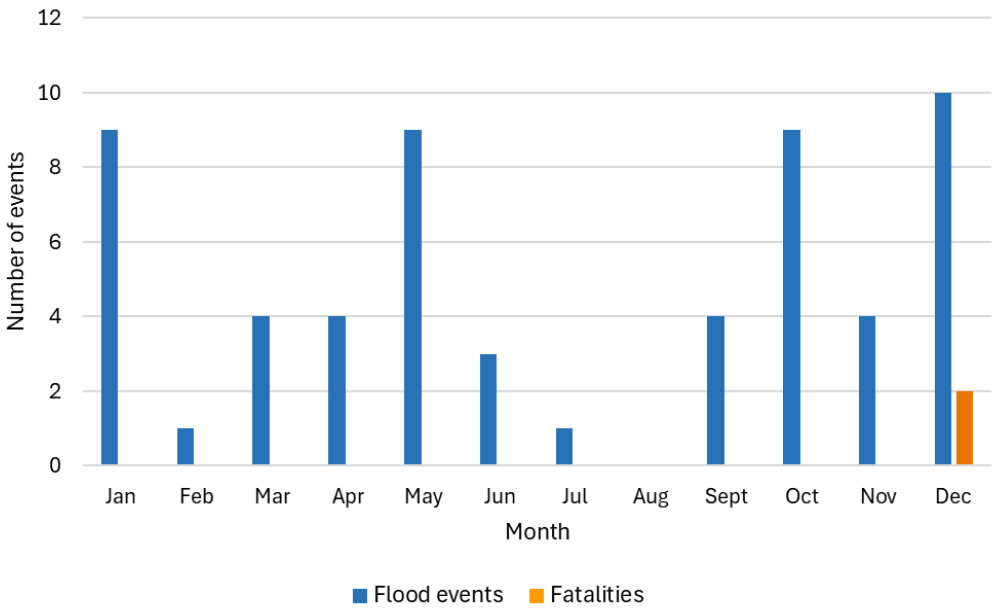

Figure 9. Monthly distribution of flood events affecting Nicosia wider region during the study period.

 doi:10.20944/preprints202605.1112.v1

To investigate the distribution of flood events by impact severity (I) across the three weather intensity levels (W), 47 of the 58 flood events recorded in the Nicosia urban area were analyzed. This restriction reflects limitations in rainfall data availability for some peri-urban and rural areas during the early part of the study period. The resulting distribution is presented in both absolute numbers and percentages in Figures 10a and 10b, respectively. Events classified under low weather intensity (W1) are predominantly associated with low impact severity (I1), accounting for 58% of cases. However, a substantial proportion (42%) of W1 events are associated with moderate impact severity (I2), highlighting the pronounced vulnerability of Nicosia's urban infrastructure even to lower-intensity rainfall events. Flood events occurred under moderate weather-intensity (W2) have reported impacts across all severity levels (I1, I2, and I3), with 4, 2, and 1 events, respectively. High weather-intensity events (W3) tend to be associated with more severe impacts. Among the four W3 events, two resulted in moderate impacts (I2), one in high impact (I3), and one in low impact (I1). Notably, unlike the Chania region where I3 impacts were exclusively tied to W3 conditions, in Nicosia, high-severity impacts occur under both W2 and W3 categories. This indicates that, although high-intensity rainfall remains a primary driver, flood severity is largely controlled by the interaction between precipitation intensity and urban surface characteristics, particularly the capacity and condition of the urban drainage system. Overall, the observed flood characteristics in Nicosia are consistent with anthropogenic and land-use-driven hazard patterns across the urban area. In environments such as the Pediaios basin, the combination of extensive impervious surfaces and the encroachment of built infrastructure onto the natural floodplain promotes a rapid hydrological response. This contrasts with terrain-driven responses in the mountainous catchment of Koiliaris basin. In Nicosia, flood hazard is instead primarily controlled by urban runoff processes and the efficiency of the drainage system, rather than by geomorphological factors.

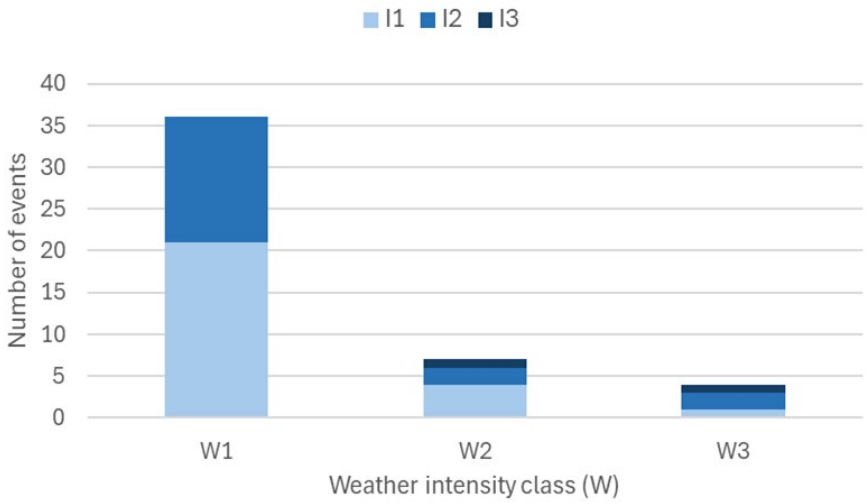

Figure 10. a. Number of flood events in Nicosia distributed by impact severity (I) within each weather intensity class (W) for Nicosia urban area.

 doi:10.20944/preprints202605.1112.v1

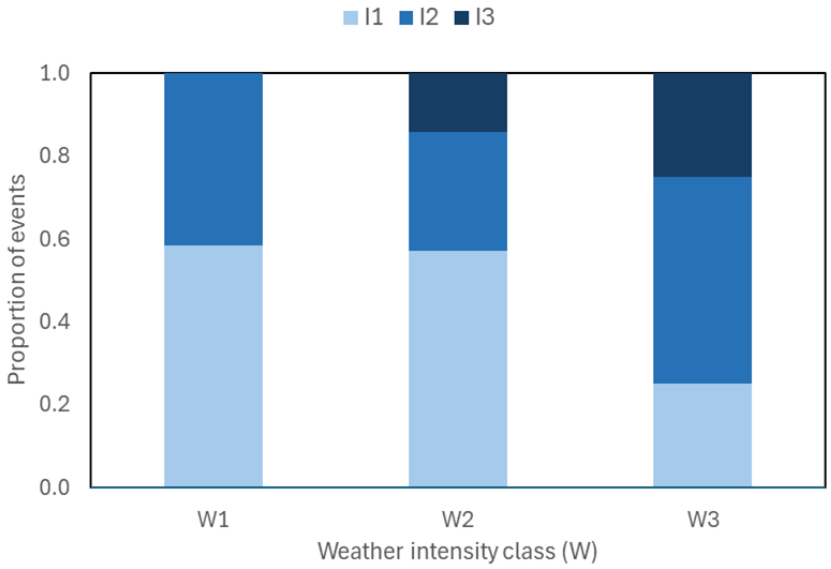

Figure 10. b. Distribution of flood events by impact severity (I) within each weather intensity class (W) for Nicosia urban area.

Table 3. Flood events that affected Nicosia District in 2000-2025. Data include date, reference location, impact severity (I), and a brief description of reported impacts (source: Cyprus WDD).

Date	Reference Area	I	Description
27/9/2000	Nicosia	1	30-min intense rain flooded houses and roads in 5 Nicosia districts.
9/10/2000	Alambra	1	Two buses trapped in flooded underpasses; houses and lands flooded in Dali/Alambra.
28/11/2000	Mandria, Lakatamia, Latsia, Psimolofou, Geri	2	Flooding of bridge in Mandria caused severe highway flooding. Critical crop/tree damage in Mandria, flooding of a furniture factory in Latsia, and widespread flooding of houses, basements, and shops across several Nicosia districts and Limassol.
13/3/2001	Strovolos, Engomi, Archangelos, Kato Moni, Meniko	1	Sudden downpour flooded buildings/roads; 150 Fire Dept calls; kindergarten evacuated; car swept away by rushing waters in Kato Moni.
19/3/2001	Nicosia	1	NA
14/5/2001	Nicosia, Strovolos, Engomi, Lakatamia, Archangelos, Tseri	2	Widespread flooding of houses and roads, the Nicosia General Hospital (wards/operating rooms), the Ministry of Interior, and immigration offices. Pediaios River overflowed, trapping cars and endangering four people near Archangelos High School. Over 100 Fire Department calls recorded.
8/12/2001	Nicosia, Potamia, Lakatamia, Strovolos, Mandria, Dali, Agios Ioannis Maloundas, Lythrodontas	2	Widespread flooding of houses and roads across. Vehicles were swept away by river waters in Dali, Agios Ioannis Malountas, and by the Gialias River in Lythrodontas, requiring emergency rescues. Over 260 Fire Department calls were recorded due to flooded properties and submerged bridges.
14/5/2002	Strovolos, Engomi, Aglantzia, Nicosia, Latsia	1	Widespread flooding across several Nicosia districts, including residential areas and the Agios Dometios hippodrome. The Fire Department responded to over 200 calls for assistance.
3/12/2002	Nicosia, Agios Dometios, Anthoupoli, Strovolos	1	Closure of major Nicosia road avenues. Key infrastructure impacts included the closure of Eleftherias Square and the General Hospital area, an impassable road at Anthoupolis-Agioi Trimithias, and the overflow of the Pedieos bridge on Alexandroupoleos Street.
31/5/2003	Strovolos, Aglantzia, Agioi Omologites	2	Flooding roads, houses, churches, and premises in record time. Akadimias park was flooded. The Nicosia-Limassol road was flooded, and the highway at the Strovolos roundabout converted to lake.

 doi:10.20944/preprints202605.1112.v1

Date	Reference Area	I	Description
2/12/2003	Dali, Nisou, Dali, Strovolos, Lakatamia	3	Almyros River overflowed at a bridge in the Dali industrial area and near the old city hall. A driver died when the overflowing river swept his car off a bridge. Flooding on Nissou-Dali Road, the Pedieos River bridge at Strovolos in Klimataria and a bridge in Lakatamia on Kapodistria Street (the bridge was damaged as well due to the flooding).
4/12/2003	Nicosia, Latsia, Tseri	1	The Ministry of Education and warehouses in Latsia flooded. Many cars were immobilized at major roundabouts and intersections; roads and premises in Nicosia, Latsia, Geri, and Agios Antonis were flooded.
12-13/12/2003	Nicosia. Strovolos, Archangelos, Dali, Nisou, Paleometocho, Agioi Trimithias	3	Pedieos, Gialias, and Kouti Rivers overflowed. Flooding of streets, homes, and garages across Nicosia, Larnaca, and Limassol. Multiple bridges overflowed, collapsed, or were severed; debris blocked river channels, and a school bus driver drowned after his vehicle was swept away in Pera Chorio Nissos. Military vehicles were swept away, several roads collapsed, and drivers were trapped in their vehicles.
11/1/2004	Nicosia, Kato Moni, Agia Marina Xyliatou	1	Flooded basements and properties in Nicosia, leaving four homes uninhabitable. Major roads, underpasses, and a section of the Limassol-Nicosia highway were closed due to water accumulation. Drivers were towed from flooded avenues, and the Kato Moni-Agia Marina road closed after a bridge overflowed.
31/5-1/6/2005	Aglantzia, Lakatamia, Strovolos, Engomi, Ergates, Kampia, Psimolofou, Deftera, Pera Oreinis, Agioi Trimithias, Arediou, Paleometocho	3	Pedieos River overflowed, sweeping away multiple bridges. Significant infrastructure damaged, including collapsed roads, cracked pavement, and flooded highways (Nicosia-Limassol and Larnaca-Kalo Chorio). Numerous homes, shops, and government offices were flooded, many drivers were trapped in flooded roads and ditches across Nicosia, Lakatamia, and Larnaca.
27/3/2006	Strovolos, Engomi, Aglantziam Agioi Omologites, Akropoli, Archangelos	1	Flooded roads across Nicosia, Strovolos, and Aglantzia. Parked cars at the University of Cyprus were swept away, a truck was trapped by an overflowing river near Omorfita, and part of the road surface on Louki Akrita Street was displaced.
5/7/2006	Strovolos, Engomi, Aglantzia, Agioi Omologites, Akropoli, Archangelos	1	Flooded streets and properties.
22/10/2008	Nicosia, Aglantzia, Strovolois, Archangelos	1	Flooded roads and basements. Streets in Archangelos were closed, and construction on Stadiou Street led to cars being trapped in floodwaters. Major junctions near Nikis Avenue were flooded.
27/10/2009	Alambra, Agia Varvara, Nisou, Lymbia, Dali	3	Large areas flooded. The Gialias and Geros Rivers overflowed, and the Lymbia Dam spilled over, closing the Nicosia-Limassol highway and several regional roads. In Alambra, 30 homes and businesses were destroyed, and a car was swept by floodwaters. In Pera Chorio Nisou, water levels exceeded one meter in homes, and a shoe store suffered 150,000 euros in damages.
28/10/2009	Nicosia, Engomi	1	Flooded houses and properties. Major roads were flooded.
18/1/2010	Nicosia, Choletra, Astromeritis, Peristerona, Lakatamia, Akaki, Orounda, Strovolos, Pera, Dali	2	Severe flooding across Cyprus, primarily hitting Astromeritis and Peristerona after the Komitis River overflowed, water reached 1.5 meters, trapping 10 people and damaging 87 properties. Rivers also overflowed in Limassol, Nicosia, and Paphos, closing several roads and bridges, including the Ziripilli and Pedieos bridges. In Akamas, seven tourists were stranded due to a rising tributary.
13/6/2011	Nisou, Dali, Alambra	2	Heavy flooding across Larnaca and Nicosia with many roads became impassable. In Nicosia, the Gialias River overflowed, sweeping away two vehicles and flooding homes in Dali, Alambra, and Pera Chorio

 doi:10.20944/preprints202605.1112.v1

Date	Reference Area	I	Description
			Nisou. Multiple overpasses at Kotsiatis and Tseri were closed, and the Nea Ledra area was cut off for several hours.
24/10/2012	Strovolos, Palouriotissa	2	Heavy rain caused flooding basements and homes. The Fire Department responded to 50 calls, including the rescue of two women and a child after five vehicles were swept away by a tributary of the Pedieos River near the SOPAZ roundabout.
9/5/2013	Nicosia, Lakatamia, Palouriotisa	1	A severe storm with hail caused over 60 calls for emergency assistance in Nicosia. The Fire Department and Police rescued drivers from eight incidents. Flooding occurred at the Nicosia Municipal Market and Makarios Stadium, while the tunnel beneath the Lakatamia roundabout was completely submerged.
9/12/2014	Nicosia, Latsia, Strovolos, Kokkinotrimithia, Agioi Trimithias, Mamari	1	Widespread flooding. An overflowing river near a military camp swept away cars, and Fire Department rescued several trapped drivers. In the old city, Ledra Street was completely submerged.
20/9/2015	Nicosia	1	Flooding in the Engomi and Makedonitissa areas of Nicosia. Lefkotheou Street, 28th October Street, Griva Digeni Avenue, and Ilias Papakyriakou Street was closed.
26/10/2015	Nicosia	1	Heavy rain hit Nicosia, Larnaca, and Limassol. Several homes and roads were flooded. Fire Department had 39 calls for emergency assistance.
12/4/2016	Strovolos, Lakatamia	1	Rising waters in the Pedieos River led to the closure of Great Alexander Road in Strovolos. In Lakatamia, several streets were closed, and the Fire Department and Police had to rescue students and two adults trapped inside the 5th Primary School of Agios Ioannis Chrysostomos.
10/6/2016	Latsia, Dali, Tseri	2	A sudden noon downpour caused extended flooding, triggering over 80 calls for help. In Latsia, an overflowing river swept away vehicles and trapped a group of children at a festival, requiring a Fire Department evacuation. The Latsia industrial area was submerged, and the river at Athalassa Park overflowed, flooding a pumping station and reaching the University of Cyprus sports fields.
9/2/2017	Strovolos, Lakatamia, Engomi	2	Heavy rainfall caused flooding in extended areas in Nicosia, Lakatamia and the surrounding highway. Key bridges over the Pedieos River (Alexandroupolis and Erythrou Stavrou) were closed, and 28 October Avenue in Engomi was completely submerged. Fire Department rescued a woman trapped in her car on Iosif Hatziosif Avenue and a mother with her child trapped on the Pediou Bridge.
29/5/2018	Akaki, Peristerona	1	Flooding reported in Akaki-Peristerona area. The Serrachi River overflowed, forcing the closure of the main road between the two communities and the flooding of 19 properties.
30/5/2018	Nicosia, Meniko	1	Heavy rainfall caused the Serrachi River to overflow, forcing the closure of Agios Kyprianou Street in Meniko. In Nicosia, several main roads flooded, with Tseriou Avenue being particularly affected.
31/5/2018	Lakatamia	1	Many road in Lakatamia, Anthoupoli, Anageia, and Deftera flooded. Agios Georgios Street became impassable due to massive water accumulation. The Fire Department responded to 30 calls for water pumping, and a specialized EMAK team performed two rescues of drivers trapped in their vehicles in Anthoupoli.
30/9/2018	Engomi, Strovolos, Lakatamia, Palouriotissa, Kaimakli, Aglantzia, old Nicosia	2	Heavy rain and hail hit Nicosia. The Fire Department responded to 70 calls, including towing two trapped vehicles and removing numerous fallen trees from roadways and parked cars. Major flooding was reported on Digenis Akritas, Prodromou, and Athalassis Avenue, while crews worked extensively to clear blocked storm drains across the capital.
20/10/2018	Kakopetria, Alambra	3	Extreme rainfall of 76 mm in one hour caused devastating flooding in the Platania area of Kakopetria. The restaurants “Prasini Koilada,”

 doi:10.20944/preprints202605.1112.v1

Date	Reference Area	I	Description
			"Riviera," and "Droseri Potamia" were submerged, and the Cyprus Scouts' campsite was flooded. Debris and landslides blocked main roads and destroyed a stream-bed path, while the Argaki-Karvounas hydrometric station recorded its highest flow since 1966. In Alambra, the road network beneath the highway was transformed into a river.
21/10/2018	Kokkinotrimithia, Paleometocho, Nicosia, Lakatamia, Strovolos	1	Heavy rain flooded several areas. The Fire Department responded to over 180 calls for water pumping and driver rescues. The underpass at the METRO roundabout in Strovolos was closed due to extreme water accumulation, and numerous roads became dangerously slippery.
29/11/2018	Kaimakli	1	Storm "Penelope" flooded Nicosia, the Fire Department rescued a person trapped in a car on Agios Hilarionos Avenue in Kaimakli using an excavator and unbloched two parked cars.
4/12/2018	Nicosia, Strovolos, Aglantzia, Latsia, Dali	2	A hailstorm turned Nicosia's streets into rivers, flooding areas from Faneromeni to Latsia. The Katevas River overflowed, submerging Larnacos Avenue under half a meter of water and flooding shops and garages. The Famagusta Gate and "Melina Merkouri" Hall suffered unprecedented damage, while water reached one meter deep in Pallouriotissa, flooding homes. Fire Department rescued trapped drivers and pumping water from basements across Engomi, Strovolos, and Aglantzia.
15/01/2019	Ayia Marina Xyliatou, Peristerona, Akaki	1	Flooding caused roads closed in Agia Marina Xyliato to Agia Marina fence, due to overflow of the fence. Old Agia Marina – Peristerona road, and main road to Akaki closed due to overflow of the river.
16/01/2019	Lakatamia, Strovolos, Deftera	1	Due to the overflow of the Pedieos River many roads were closed, and emergency rescues were reported in the affected regions.
16/01/2019	Dali, Pera, Kotsiatis, Ayia Varvara, Alambra, Potamia	1	The Gialias River overflowed, closing key roads in Pera Chorio, Dali, and Potamia. Emergency crews rescued three people.
16/06/2019	Nicosia, Strovolos, Lakatamia, Latsia, Engomi	1	Flooded properties and roads caused by heavy rainfall and strong winds in the wider Nicosia urban area. Pediaios overflowed causing flooding of the bridge on Alexandroupoleos Street.
20/10/2019	Strovolos, Lakatamia, Engomi, Latsia	1	Severe flooding prompted 73 emergency calls to the Fire Department. The bridge on Alexandroupoleos Street, and the bridge on I. Kapodistria Street in Lakatamia were closed due to the overflow of the Pedieos River.
27/10/2019	Nicosia, Strovolos, Palouriotissa Aglantzia, Latsia	2	A severe one-hour storm involving heavy rain and hail caused extensive flooding across Nicosia, prompting 180 emergency calls. In the city center and SOPAZ area, the overflow of the Katevas River flooded homes and businesses, trapping several individuals inside premises. Major arteries, including the Nicosia–Limassol highway and Limassol Avenue, became impassable due to significant water accumulation, resulting in dozens of immobilized vehicles and flooded underground structures in Strovolos and Aglantzia.
07/01/2020	Deftera, Lakatamia, Strovolos,	1	The Pedieos River overflowed, flooding the Panagia Chrysospiliotissa cave square in Kato Deftera and closing the main access road. Multiple bridges were submerged, forcing the closure of key roads including Alexandroupoleos (Strovolos), Erythrou Stavrou (Presidential Palace area), and local routes in Lakatamia, Deftera, and Ergates.
07/01/2020	Potamia, Dali, Nisou, Ayia Varvara, Kotsiatis	1	The Gialias River overflowed multiple bridges, forcing the closure of key roads in Pera Chorio, Dali, Potamia, and the Kotsiatis-Agia Varvara route. Affected infrastructure included streets near the Chalkanora stadium and local cemeteries, causing significant regional traffic disruption.
05/05/2020	Engomi, Strovolos	2	The overflow of the Klimos River in the Agios Dometios buffer zone caused significant property damage. Debris obstructed drainage systems, exacerbating the flooding of homes in Engomi and rendering residential streets in Strovolos impassable. Fire Department

 doi:10.20944/preprints202605.1112.v1

Date	Reference Area	I	Description
			interventions needed to rescue property and mitigate public safety risks across the impacted municipalities.
30/12/2021	Strovolos, Lakatamia, Engomi	2	The overflow of the Pedieos River and widespread flooding led to the rescue of twelve individuals from submerged vehicles and residences by the Fire Department and Civil Defense. Emergency crews performed critical water pumping at homes, a nursing home, and the Mennoia detention center. Significant road closures occurred in Strovolos and Lakatamia, a rescue from the riverbed, while the Nicosia–Limassol highway saw ten weather-related traffic accidents and extensive flooding.
23/01/2022	Nicosia, Latsia,, Dali	2	In the wider Nicosia district, significant agricultural damage occurred as fields were submerged and acres of crops were destroyed by mud and standing water. In Latsia, heavy rain turned roads into rivers and flooded residential areas.
29/04/2023	Nicosia	2	Severe weather in Nicosia prompted 29 emergency interventions, including 14 for fallen trees, 15 for water pumping from flooded properties and rescued drivers trapped at flooded roads. The storm caused significant damages to the electricity network.
14/11/2023	Geri, Latsia, Dali	1	Severe flooding in the Geri Industrial Area transformed roads into rivers, immobilizing traffic and trapping two workers in a factory who were rescued by the Fire Department. In Idalion, emergency crews conducted three pumping operations in flooded underground premises.
18/03/2024	Strovolos, Aglantzia, Tseri, Latsia	1	Multiple roads, including Limassol Avenue, were closed due to dangerous conditions and widespread vehicle immobilizations, while significant damage was reported to various commercial and residential premises. 78 emergency interventions across Nicosia were reported.
09/01/2024	Dali	1	In Dali and Southern Nicosia, heavy rainfall caused localized flooding of properties and drainage failures. The Fire Service responded to several calls for water pumping from basements, and police monitored rural roads for mud and debris.
09/04/2024	Ayia Varvara, Dali, Aglantzia	2	A sudden overflow of the Pedieos River caused rapid flooding across Strovolos, Dali, and Tseri, damaging infrastructure. In Tseri, floodwaters completely submerged a residential basement to ceiling level. The Fire Department responded to 30 calls in Nicosia for water pumping and vehicle recoveries, including a critical rescue by Police in Nea Ledra, where three people were trapped in a vehicle on a flooded bridge. The storm triggered widespread power outages in Palaichori and surrounding rural communities.
23/09/2024	Engomi, Strovolos, Aglanzia	1	Localized flooding, where inadequate drainage systems caused roads to become briefly impassable. The Fire Department responded to approximately 12 incidents.
04/04/2025	Archangelos, Engomi, Tseri, Paleometocho	1	Severe weather triggered 22 emergency interventions across Archangelos, Makedonitissa, Engomi, Tseri, and Paliometochos. A lightning strike also severed a utility pole.
12/11/2025	Lakatamia, Strovolos, Palouriotisa	2	Heavy rain caused serious problems on the road network, flooding, power outages and multiple calls to the Fire Department. The Fire Department responded to over 100 incidents, the majority of which involved water pumping, immobilised vehicles, fallen trees and incidents that affected the safety of drivers and students, Bridges overflowed and roads were closed in Alexandroupoli and Erithrou Stavrou.
9-10/12/2025	Strovolos, Latsia, Nicosia	2	Storm Byron persistent caused the Pedieos River to overflow, flooding main roads and underpasses in Strovolos and Latsia. The Fire Department responded to dozens of calls to pump water from residential and commercial basements. Police reported multiple vehicle recoveries and landslides on connecting mountain routes.

 doi:10.20944/preprints202605.1112.v1

Date	Reference Area	I	Description
			Significant infrastructure disruption occurred across the Nicosia district, including widespread power outages in many regions.

4. Discussion

The results of the FHI analysis reveal distinct flood-generating mechanisms between the two Mediterranean catchments, reflecting the contrasting influence of geomorphological and anthropogenic controls on hydrological response. By integrating topographic, hydrological, and climatological indicators within an AHP-based multi-criteria framework, the methodology successfully captures the spatial variability of flood-prone areas in both the Koiliaris and Pediaios basins. The consistency between the modeled hazard patterns and the historical flood-event analysis further supports the robustness of the proposed approach and highlights its applicability for flood hazard assessment in heterogeneous Mediterranean environments.

The contrasting results between the two catchments demonstrate the versatility and regional adaptability of the AHP method. In the Koiliaris basin, flood hazard is primarily terrain-driven, where the Topographic Wetness Index (TWI) acts as the principal determinant of lowland water accumulation and the spatial distribution of runoff-prone areas. The elevated hazard levels identified along the downstream alluvial plains, and river corridors reflect the geomorphological structure of the basin, where steep mountainous slopes in the upstream region promote rapid runoff generation that subsequently converges in low-gradient accumulation zones. This pattern is consistent with the historical flood-event analysis, which showed that the most severe flood impacts in Chania were associated with locations characterized by high topographic convergence and rapid hydrological response. The alignment between high-severity historical events and the modeled “High” and “Very High” hazard classes confirms that the FHI effectively captures the hydro-geomorphological controls governing flood generation in mountainous Mediterranean catchments. In contrast, the Pediaios basin exhibits a flood hazard regime dominated by anthropogenic drivers. Here, the relatively high weighting of the Curve Number (CN; 0.40) effectively captures the increased vulnerability associated with rapid urbanization and the expansion of impervious surfaces within the Nicosia metropolitan area. The resulting hazard patterns highlight the downstream urban corridor of the basin as the most flood-prone sector, where reduced infiltration capacity and accelerated surface runoff substantially modify the natural hydrological response of the watershed. Historical flood events in Nicosia further support this interpretation, as the most severe impacts consistently occurred in densely urbanized districts characterized by extensive surface impermeability and limited drainage capacity. In this context, flood generation is controlled less by natural terrain morphology and more by human-induced land-cover change and urban runoff processes. The results therefore demonstrate how urbanization can fundamentally alter Mediterranean basin hydrology, shifting the dominant flood-generating mechanism from geomorphological controls toward anthropogenic surface modification.

The distinction between natural and anthropogenic flood drivers is further clarified through the statistical classification framework used to define the hazard levels. The application of the Natural Breaks (Jenks) classification method proved essential for establishing statistically meaningful hazard thresholds in both catchments. By minimizing variance within classes while maximizing variance between classes, the method successfully isolated the most hydrologically critical zones. In the Koiliaris basin, the classification emphasizes the mountainous runoff-contributing areas and downstream accumulation plains that characterize rapid runoff concentration in steep Mediterranean terrain. In the Pediaios basin, the classification effectively distinguishes the highly urbanized sectors of Nicosia, where flood hazard is intensified by elevated runoff coefficients, high surface impermeability, and drainage accumulation along the urban river network. The resulting spatial hierarchy provides a clear distinction between moderate- and high-hazard zones and therefore supports the identification of priority areas for flood-risk management and urban planning interventions.

 doi:10.20944/preprints202605.1112.v1

The integration of the R20 precipitation index as a climatological modulator further strengthens the physical interpretation of the FHI. Although assigned the lowest weight in the AHP framework (0.15), the R20 index provides the meteorological forcing necessary to constrain the hydrological susceptibility represented by TWI and CN. In both basins, the inclusion of R20 ensures that the final hazard patterns are linked not only to terrain and land-surface characteristics but also to the spatial frequency of heavy rainfall events capable of triggering flooding. This interaction between terrain susceptibility and extreme precipitation forcing is particularly evident in the historical-event analysis. In Chania, the most severe flood impacts were associated exclusively with the highest weather-intensity category (W3), indicating that extreme rainfall acts as the principal trigger within a geomorphologically sensitive environment. In Nicosia, however, severe impacts were observed under both W2 and W3 conditions, suggesting that urban surface characteristics and drainage limitations can amplify flood impacts even under less extreme meteorological forcing. These findings highlight the importance of considering both climatic triggers and basin-specific hydrological response mechanisms when assessing flood hazard in Mediterranean environments.

The historical flood-event analysis also demonstrates the value of integrating empirical impact information with spatial susceptibility modelling. The agreement between documented flood impacts and the modeled hazard zones supports the reliability of the FHI as a tool for identifying areas exposed to recurrent flooding. The temporal analysis of flood occurrence reveals increasing event frequency in both regions during the last decade of the study period, particularly after the mid-2010s. Although part of this increase may reflect improvements in reporting and documentation practices, it is also consistent with evolving hydroclimatic conditions, including increased precipitation variability and more frequent high-intensity rainfall events in the Eastern Mediterranean.

Beyond these interannual patterns, the seasonal distribution of flood events provides additional insight into the underlying flood-generating mechanisms and helps explain the observed regional differences. In Chania, flood occurrence is strongly concentrated in autumn, extending into winter, reflecting the dominance of intense frontal systems and orographic rainfall in mountainous Mediterranean environments. This pattern indicates that flooding is mainly controlled by the wet season, when repeated heavy rainfall events lead to multiple flood responses. In contrast, Nicosia exhibits a more dispersed seasonal signal, with elevated flood activity extending from autumn through spring. This reflects the combined influence of synoptic systems and short-duration convective storms, which are typical of semi-arid inland Cyprus. As a result, flooding is not confined to a single wet season but can occur under different rainfall types across a wider part of the year, explaining the higher number of flood events and the more distributed temporal pattern of flood occurrence in this region.

5. Conclusions

Future development of the proposed multi-indicator flood hazard framework involves its integration with hydrodynamic and forecasting systems. Linking it with operational platforms such as the MedGIFORS (Medicane GNSS-based Impact Forecasting and Emergency Management System) initiative could enhance early warning capabilities through high-resolution GNSS-derived atmospheric data and real-time impact forecasting. This would support a transition from static hazard mapping to dynamic, near-real-time flood risk assessment and decision support. Coupling physically based modelling with operational forecasting and emergency management systems would therefore improve the practical value of the framework for flood risk reduction and resilience planning in Mediterranean catchments.

Author Contributions: Conceptualization, V.K., C.L., D.G., C.O., H.H.; methodology, A.B., V.K., K.P., D.G.; model development, A.B., V.K.; validation, A.B., D.G., V.K.; formal analysis, D.G.; data curation, D.G. A.B, K.P; writing—original draft preparation, D.G.; writing—review and editing, D.G., A.B., V.K., C.O.; supervision, H.H.,

 doi:10.20944/preprints202605.1112.v1

C.L.; project administration, C.O.; funding acquisition, C.O, H.H. All authors have read and agreed to the published version of the manuscript.

Funding: This research is conducted within MedGIFORS project (Project Protocol Number: BRIDGE2HORIZON/0823D/0011) which is within the framework of the «RESTART 2016-2020» Programmes for Research, Technological Development and Innovation (RTDI) which is co-financed by the Republic of Cyprus and the European Regional Development Fund.

Data Availability Statement: The data support the findings of this study are available from the authors upon reasonable request. Access may be granted under appropriate data-use conditions and in accordance with applicable intellectual property rights, confidentiality obligations, and restrictions arising from ongoing funded research projects.

Acknowledgments: The authors would like to thank Mrs Georgia Georgoiou – Hydrologist from the Cyprus Water Development Department for the provision of historical flood data for Cyprus.

Conflicts of Interest: The authors declare no conflicts of interest.

Abbreviations

The following abbreviations are used in this manuscript:

AHP	Analytic Hierarchy Process
CERRA	Copernicus European Regional Reanalysis for Europe
CLC	CORINE Land Cover
CN	Curve Number
CORINE	Coordination of Information on the Environment
DEM	Digital Elevation Model
DoM	Department of Meteorology (Cyprus
ESDAC	European Soil Data Centre
ETCCDI	Expert Team on Climate Change Detection and Indices
EU-DEM	European Digital Elevation Model
FHI	Flood Hazard Index
GIS	Geographic Information Systems
HIWE-DB	High-Impact Weather Events Database
HSG	Hydrologic Soil Groups
I	Impact Severity
LULC	Land Use / Land Cover
MCDA	Multi-Criteria Decision Analysis
METEO	Meteorological Unit at the National Observatory of Athens
R20	Heavy rainfall frequency index
TWI	Topographic Wetness Index
USDA-NRCS	United States Department of Agriculture - Natural Resources Conservation Service
USDA-SCS	United States Department of Agriculture - Soil Conservation Service
W	Weather Intensity
WDD	Water Development Department (Cyprus)

References

1. Kundzewicz, Z.W.; et al. Flood risk and climate change: Global and regional perspectives. Hydrol. Sci. J. 2013, 59, 1–28. https://doi.org/10.1080/02626667.2013.857411.
2. Hirabayashi, Y.; Mahendran, R.; Koirala, S.; et al. Global flood risk under climate change. Nat. Clim. Chang. 2013, 3, 816–821. https://doi.org/10.1038/nclimate1911.
3. Jongman, B.; Ward, P.J.; Aerts, J.C.J.H. Global exposure to river and coastal flooding: Long term trends and changes. Glob. Environ. Chang. 2012, 22, 823–835. https://doi.org/10.1016/j.gloenvcha.2012.07.004.
4. Savari, M.; Jafari, A.; Sheheytavi, A. Determining factors affecting flood risk perception among local communities in Iran. Sci. Rep. 2025, 15, 4076. https://doi.org/10.1038/s41598-025-88673-2.

 doi:10.20944/preprints202605.1112.v1

5. Peiris, M.T.O.V.; Randeniya, N.; Bopitiyegedara, N. How do anthropogenic factors define flood risk perception of vulnerable communities? Evidence from Kelani River Lower Basin, Colombo, Sri Lanka. Int. J. Disaster Risk Reduct. 2025, 120, 105352. https://doi.org/10.1016/j.ijdrr.2025.105352.
6. Raphela, T.D.; Matsididi, M. The causes and impacts of flood risks in South Africa. Front. Water 2025, 6, 1524533. https://doi.org/10.3389/frwa.2024.1524533.
7. Michaelides, S.; Karacostas, T.; Sánchez, J.L.; Retalis, A.; Pytharoulis, I.; Homar, V.; Romero, R.; Zanis, P.; Giannakopoulos, C.; Bühl, J.; Ansmann, A.; Merino, A.; Melcón, P.; Lagouvardos, K.; Kotroni, V.; Bruggeman, A.; López-Moreno, J.I.; Berthet, C.; Katragkou, E.; Tymvios, F.; Hadjimitsis, D.G.; Mamouri, R.-E.; Nisantzi, A. Reviews and perspectives of high-impact atmospheric processes in the Mediterranean. Atmos. Res. 2018, 208, 4–44.
8. Tramblay, Y.; Arnaud, P.; Artigue, G.; Lang, M.; Paquet, E.; Neppel, L.; Sauquet, E. Changes in Mediterranean flood processes and seasonality. Hydrol. Earth Syst. Sci. 2023, 27, 2973–2987. https://doi.org/10.5194/hess-27-2973-2023.
9. Diakakis, M.; Papagiannaki, K.; Fouskaris, M. The occurrence of catastrophic multiple-fatality flash floods in the Eastern Mediterranean region. Water 2023, 15, 119. https://doi.org/10.3390/w15010119.
10. Papagiannaki, K.; Lagouvardos, K.; Kotroni, V. A database of high-impact weather events in Greece: A descriptive impact analysis for the period 2001–2011. Nat. Hazards Earth Syst. Sci. 2013, 13, 727–736. https://doi.org/10.5194/nhess-13-727-2013.
11. Papagiannaki, K.; Lagouvardos, K.; Kotroni, V.; Bezes, A. Flash flood occurrence and relation to the rainfall hazard in a highly urbanized area. Nat. Hazards Earth Syst. Sci. 2015, 15, 1859–1872. https://doi.org/10.5194/nhess-15-1859-2015.
12. Papagiannaki, K.; Kotroni, V.; Lagouvardos, K. Insights from the High-Impact Weather Events Database (HIWE-DB). Climate 2026, in press.
13. Hosseiny, H.; Nazari, F.; Smith, V.; et al. A framework for modeling flood depth using a hybrid of hydraulics and machine learning. Sci. Rep. 2020, 10, 8222. https://doi.org/10.1038/s41598-020-65232-5.
14. Saksena, S.; Merwade, V.; Singhofen, P.J. Flood inundation modeling and mapping by integrating surface and subsurface hydrology with river hydrodynamics. J. Hydrol. 2019, 575, 1155–1177. https://doi.org/10.1016/j.jhydrol.2019.06.024.
15. Teng, J.; Jakeman, A.J.; Vaze, J.; Croke, B.F.W.; Dutta, D.; Kim, S. Flood inundation modelling: A review of methods, recent advances and uncertainty analysis. Environ. Model. Softw. 2017, 90, 201–216. https://doi.org/10.1016/j.envsoft.2017.01.006.
16. Kader, Z.; Islam, M.R.; Aziz, M.T.; et al. GIS and AHP-based flood susceptibility mapping: A case study of Bangladesh. Sustain. Water Resour. Manag. 2024, 10, 170. https://doi.org/10.1007/s40899-024-01150-y.
17. Ahmed, A.; Al Maliki, A.; Hashim, B.; et al. Flood susceptibility mapping utilizing the integration of geospatial and multivariate statistical analysis, Erbil area in Northern Iraq as a case study. Sci. Rep. 2023, 13, 11919. https://doi.org/10.1038/s41598-023-39290-4.
18. Fenglin, W.; Ahmad, I.; Zelenakova, M.; et al. Exploratory regression modeling for flood susceptibility mapping in the GIS environment. Sci. Rep. 2023, 13, 247. https://doi.org/10.1038/s41598-023-27447-0.
19. Costache, R.; Pham, Q.B.; Sharifi, E.; Linh, N.T.T.; Abba, S.I.; Vojtek, M.; Vojteková, J.; Nhi, P.T.T.; Khoi, D.N. Flash-flood susceptibility assessment using multi-criteria decision making and machine learning supported by remote sensing and GIS techniques. Remote Sens. 2020, 12, 106. https://doi.org/10.3390/rs12010106.
20. Kazakis, N.; Kougias, I.; Patsialis, T. Assessment of flood hazard areas at a regional scale using an index-based approach and Analytical Hierarchy Process: Application in Rhodope–Evros region, Greece. Sci. Total Environ. 2015, 538, 555–563. https://doi.org/10.1016/j.scitotenv.2015.08.055.
21. Alafostergios, N.; Evelpidou, N.; Spyrou, E. Flood susceptibility assessment based on the Analytical Hierarchy Process (AHP) and Geographic Information Systems (GIS): A case study of the broader area of Megala Kalyvia, Thessaly, Greece. Information 2025, 16, 671. https://doi.org/10.3390/info16080671.
22. Ashfaq, S.; Tufail, M.; Niaz, A.; Muhammad, S.; Alzahrani, H.; Tariq, A. Flood susceptibility assessment and mapping using GIS-based analytical hierarchy process and frequency ratio models. Glob. Planet. Chang. 2025, 251, 104831. https://doi.org/10.1016/j.gloplacha.2025.104831.

 doi:10.20944/preprints202605.1112.v1

23. Bouchikhi, S.; Chourak, M.; Boushaba, F.; El Baida, M. Flood susceptibility mapping in urban areas based on analytical hierarchy process: A decade-long systematic literature review. J. Afr. Earth Sci. 2026, 233, 105903. https://doi.org/10.1016/j.jafrearsci.2025.105903.
24. Beven, K.J.; Kirkby, M.J. A physically based, variable contributing area model of basin hydrology. Hydrol. Sci. J. 1979, 24, 43–69. https://doi.org/10.1080/02626667909491834.
25. Tarboton, D.G. A new method for the determination of flow directions and upslope areas in grid digital elevation models. Water Resour. Res. 1997, 33, 309–319. https://doi.org/10.1029/96WR03137.
26. Moore, I.D.; Grayson, R.B.; Ladson, A.R. Digital terrain modelling: A review of hydrological, geomorphological, and biological applications. Hydrol. Process. 1991, 5, 3–30. https://doi.org/10.1002/hyp.3360050103.
27. Tehrany, M.S.; Pradhan, B.; Jebur, M.N. Flood susceptibility mapping using a novel ensemble weights-of-evidence and support vector machine models in GIS. J. Hydrol. 2014, 512, 332–343. https://doi.org/10.1016/j.jhydrol.2014.03.008.
28. Hu, S.; Fan, Y.; Zhang, T. Assessing the effect of land use change on surface runoff in a rapidly urbanized city: A case study of the central area of Beijing. Land 2020, 9, 17. https://doi.org/10.3390/land9010017.
29. Xing, H.; Fang, K.; Yao, Q.; Zhou, F.; Ou, T.; Liu, J.; Zhou, S.; Jiang, S.; Chen, Y.; Bai, M.; Chen, J.M. Impacts of changes in climate extremes on wildfire occurrences in China. Ecol. Indic. 2023, 157, 111288. https://doi.org/10.1016/j.ecolind.2023.111288.
30. Gao, G.; Li, J.; Feng, P.; Liu, J.; Wang, Y. How extreme hydrological events correspond to climate extremes in the context of global warming: A case study in the Luanhe River Basin of North China. Int. J. Climatol. 2024, 44, 2391–2405. https://doi.org/10.1002/joc.8459.
31. Zittis, G.; Bruggeman, A.; Camera, C. 21st century projections of extreme precipitation indicators for Cyprus. Atmosphere 2020, 11, 343. https://doi.org/10.3390/atmos11040343.
32. Lagouvardos, K.; Dafis, S.; Kotroni, V.; Kyros, G.; Giannaros, C. Exploring recent (1991–2020) trends of essential climate variables in Greece. Atmosphere 2024, 15, 1104. https://doi.org/10.3390/atmos15091104.
33. Kotroni, V.; Bezes, A.; Dafis, S.; Founda, D.; Galanaki, E.; Giannaros, C.; Giannaros, T.; Karagiannidis, A.; Koletsis, I.; Kyros, G.; Lagouvardos, K.; Papagiannaki, K.; Papavasileiou, G. Long-term statistical analysis of severe weather and climate events in Greece. Atmosphere 2025, 16, 105. https://doi.org/10.3390/atmos16010105.
34. Kourgialas, N.N.; Karatzas, G.P. A national scale flood hazard mapping methodology: The case of Greece—Protection and adaptation policy approaches. Sci. Total Environ. 2017, 601–602, 441–452. https://doi.org/10.1016/j.scitotenv.2017.05.197.
35. Giustarini, L.; Hostache, R.; Matgen, P.; Schumann, G.J.-P.; Bates, P.D.; Mason, D.C. A change detection approach to flood mapping in urban areas using TerraSAR-X. IEEE Trans. Geosci. Remote Sens. 2013, 51, 2417–2430.
36. Diakakis, M. Flood history analysis and its contribution to flood hazard assessment: The case of Marathonas, Greece. Bull. Geol. Soc. Greece 2010, 43, 1323–1334. https://doi.org/10.12681/bgsg.11308.
37. Kourgialas, N.N.; Karatzas, G.P. Flood management and a GIS modelling method to assess flood-hazard areas—A case study. Hydrol. Sci. J. 2011, 56, 212–225. https://doi.org/10.1080/02626667.2011.555836.
38. Papagiannaki, K.; Kotroni, V.; Lagouvardos, K.; Bezes, A.; Vafeiadis, V.; Messini, I.; Kroustallis, E.; Totos, I. Identification of rainfall thresholds likely to trigger flood damages across a Mediterranean region, based on insurance data and rainfall observations. Water 2022, 14, 994. https://doi.org/10.3390/w14060994.
39. Santos, P.P.; Reis, E.; Pereira, S.; Santos, M. A flood susceptibility model at the national scale based on multicriteria analysis. Sci. Total Environ. 2019, 667, 325–337. https://doi.org/10.1016/j.scitotenv.2019.02.328.
40. Nikolaidis, N.P.; Karatzas, G.P.; Kourgialas, N.N.; Giannakis, G.V.; Tsakiris, G. Hydrological processes and water balance in a Mediterranean watershed: The Koiliaris River Basin in Crete. Hydrol. Process. 2013, 27, 335–347.
41. Giannaros, C.; Galanaki, E.; Kotroni, V.; Lagouvardos, K.; Oikonomou, C.; Haralambous, H.; Giannaros, T. Pre-operational application of a WRF-Hydro-based fluvial flood forecasting system in the Southeast Mediterranean. Forecasting 2021, 3, 437–446. https://doi.org/10.3390/forecast3020026.

 doi:10.20944/preprints202605.1112.v1

42. Zachariadis, T.; Hadjinicolaou, P.; Lelieveld, J. Climate change impacts and adaptation options for Cyprus. Clim. Policy 2013, 13, 1–15.
43. Charalambous, K.; Bruggeman, A.; Bakirtzis, N.; Lange, A.M. Historical flooding of the Pedieos River in Nicosia, Cyprus. *Water Hist* **8**, 191–207 (2016). https://doi.org/10.1007/s12685-016-0162-1.
44. USDA-SCS. National Engineering Handbook Section 4: Hydrology; Soil Conservation Service, U.S. Department of Agriculture: Washington, DC, USA, 1972.
45. USDA-NRCS. National Engineering Handbook, Part 630: Hydrology, Chapter 10: Estimation of Direct Runoff from Storm Rainfall. United States Department of Agriculture, Natural Resources Conservation Service, Washington, DC, 2004.
46. Ponce, V.M.; Hawkins, R.H. Runoff curve number: Has it reached maturity? J. Hydrol. Eng. 1996, 1, 11–19.
47. Mishra, S.K.; Singh, V.P. Soil Conservation Service Curve Number (SCS-CN) Methodology; Springer: Dordrecht, The Netherlands, 2003.
48. Zhang, X.; Alexander, L.; Hegerl, G.; Jones, P.; Tank, A.; Peterson, T.; Trewin, B.; Zwiers, F. Indices for monitoring changes in extremes based on daily temperature and precipitation data. WIREs Clim. Change 2011, 2, 851–870.
49. Jenks, G.F. The data model concept in statistical mapping. Int. Yearb. Cartogr. 1967, 7, 186–190.
50. Chen, W.; Pourghasemi, H.R.; Naghibi, S.A. A comparative study of landslide susceptibility maps produced using support vector machine with different kernel functions and entropy data mining models in China. Bull. Eng. Geol. Environ. 2013, 72, 343–356. https://doi.org/10.1007/s10064-012-0410-y.
51. Papathoma-Köhle, M.; Schlögl, M.; Fuchs, S. Vulnerability indicators for natural hazards: An innovative selection and weighting approach. Nat. Hazards Earth Syst. Sci. 2019, 19, 2547–2562. https://doi.org/10.5194/nhess-19-2547-2019.
52. Saaty, T.L. The analytic hierarchy process—What it is and how it is used. Math. Model. 1987, 9, 161–176. https://doi.org/10.1016/0270-0255(87)90473-8.
53. Stefanidis, S.; Stathis, D. Assessment of flood hazard based on natural and anthropogenic factors using Analytic Hierarchy Process (AHP). Nat. Hazards 2013, 68, 569–585. https://doi.org/10.1007/s11069-013-0639-5.
54. Amaro, J.; Gayà, M.; Aran, M.; and Llasat, M. C.: Preliminary results of the Social Impact Research Group of MEDEX: the request database (2000–2002) of two Meteorological Services, Nat. Hazards Earth Syst. Sci., 10, 2643–2652, https://doi.org/10.5194/nhess-10-2643-2010, 2010.
55. Cyprus Water Development Department: https://www.moa.gov.cy/moa/wdd/wdd.nsf/index_en/index_en?opendocument
56. DoM (Cyprus): https://dom.org.cy/FORECAST/Weather_warnings_guide.pdf